

Research Articles | Neurobiology of Disease

## Age-related brain atrophy and the positive effects of behavioral enrichment in middle-aged beagles

<https://doi.org/10.1523/JNEUROSCI.2366-23.2024>

Received: 15 December 2023

Revised: 8 February 2024

Accepted: 28 February 2024

Copyright © 2024 the authors

---

*This Early Release article has been peer reviewed and accepted, but has not been through the composition and copyediting processes. The final version may differ slightly in style or formatting and will contain links to any extended data.*

**Alerts:** Sign up at [www.jneurosci.org/alerts](http://www.jneurosci.org/alerts) to receive customized email alerts when the fully formatted version of this article is published.

1 **Title Page**

2 Age-related brain atrophy and the positive effects of behavioral enrichment in middle-aged beagles

3 Abbreviated title: behavioral effects on brain atrophy in aging beagles

4 Authors:

5 Jessica A. Noche<sup>1</sup>, Hamsanandini Radhakrishnan<sup>1,2</sup>, Margo F. Ubele<sup>3</sup>, Kathy Boaz<sup>3</sup>, Jennifer L. Mefford<sup>3</sup>,  
6 Erin D. Jones<sup>3</sup>, Jessica A. Perpich<sup>3</sup>, Katie McCarty<sup>3</sup>, Beverly Meacham<sup>3</sup>, Jeffrey Smiley<sup>3</sup>, Stasia A.  
7 Bembenek Bailey<sup>3</sup>, László G. Puskás, David K. Powell<sup>3</sup>, Lorena Sordo<sup>1</sup>, Michael J. Phelan<sup>1</sup>, Christopher M.  
8 Norris<sup>3</sup>, Elizabeth Head<sup>1</sup> and Craig E.L. Stark<sup>1</sup>

9 (1)University of California, Irvine, Irvine, CA, USA, 92697

10 (2)University of Pennsylvania, Philadelphia, PA, USA, 19104

11 (3)University of Kentucky, Lexington, KY, USA, 40506

12 (4) Aperus Pharma, H-6726, Szeged, Hungary

13 Corresponding author: J.A.N. [nochej@uci.edu](mailto:nochej@uci.edu)

14 Number of pages: 43

15 Number of figures=9, tables=5, multimedia=0

16 Number of words for Abstract=156, Introduction=765, Discussion=1829

17 Conflict of interest statement: L.G.P.: personal financial interests, as he is the main shareholder of one of  
18 Aperus Pharma co Ltd's company shares.

19 **Acknowledgements:**

20 The study was supported by NIH/NIA R01AG056998 (EH/CN/CELS). JAN is supported by NIH/NIA  
21 T32AG073088. We thank Christine Lee and Elena Singh for their assistance in quality control of the  
22 imaging data.

23

24

25

26  
27  
28  
29  
30  
31  
32  
33  
34  
35  
36  
37  
38  
39  
40  
41  
42  
43  
44  
45  
46  
47  
48  
49  
50  
51  
52  
53  
54

## ABSTRACT

Aging dogs serve as a valuable preclinical model for Alzheimer's disease (AD) due to their natural age-related development of beta-amyloid (A $\beta$ ) plaques, human-like metabolism, and large brains that are ideal for studying structural brain aging trajectories from serial neuroimaging. Here we examined the effects of chronic treatment with the calcineurin inhibitor (CNI) tacrolimus or the nuclear factor of activated T cells (NFAT)-inhibiting compound Q134R on age-related canine brain atrophy from a longitudinal study in middle-aged beagles (36 females, 7 males) undergoing behavioral enrichment. Annual MRI was analyzed using modern, automated techniques for region-of-interest -based and voxel-based volumetric assessments. We found that the frontal lobe showed accelerated atrophy with age, while the caudate nucleus remained relatively stable. Remarkably, the hippocampus increased in volume in all dogs. None of these changes were influenced by tacrolimus or Q134R treatment. Our results suggest that behavioral enrichment can prevent atrophy and increase the volume of the hippocampus but does not prevent aging-associated prefrontal cortex atrophy.

**SIGNIFICANCE STATEMENT:** Aging canines naturally show significant neuropathological similarities to human aging and AD, making them valuable translational models for testing disease-modifying treatments. We applied modern, state-of-the-art longitudinal volumetric analysis approaches to evaluate treatment effects from structural MRI in a large cohort of middle-aged beagles treated with the FDA approved calcineurin inhibitor, tacrolimus, or the experimental NFAT inhibitor, Q134R, while undergoing extensive behavioral enrichment. We show increased hippocampal volumes across all dogs, even control placebo dogs, compelling evidence for a strong enrichment-related benefit on hippocampal structural integrity. Our findings are the first of its kind to demonstrate benefits of behavioral intervention on longitudinal structural brain changes in a higher mammalian model of aging and AD.

Keywords: beagle, calcineurin, Q134R, prevention, tacrolimus, Alzheimer's disease, amyloid, neurodegeneration, prevention

## 55 Introduction

56 Canines share aging-related neuropathological features with humans, making for a valuable  
57 translational model for Alzheimer's disease (AD). Aging canines intrinsically develop diffuse beta-  
58 amyloid (A $\beta$ ) pathology that is associated with cognitive decline akin to human mild cognitive  
59 impairment (MCI) (Cotman & Head, 2008). Furthermore, cognitive functions tested in beagles that are  
60 relevant in AD, including spatial memory and executive function, are vulnerable to aging and A $\beta$  burden  
61 (Chan et al., 2002; Head et al., 1998; Rofina et al., 2006; Studzinski et al., 2006; Tapp et al., 2003). Their  
62 drug tolerance and metabolism align with humans as well (Martinez et al., 2021). Furthermore, the  
63 larger, gyrencephalic brain of beagles compared to lower mammalian AD models proves advantageous  
64 for *in vivo* structural assessments with magnetic resonance imaging (MRI) and for larger sampling  
65 volumes for postmortem histological evaluations. These features, coupled with their shorter lifespans  
66 relative to humans, make them ideal for studying longitudinal effects of behavioral and pharmacological  
67 interventions (Su et al., 2005; Head et al., 2008; Araujo et al., 2022).

68 Clinical trials in AD patients often target the classic pathological hallmarks, the aggregation of A $\beta$   
69 plaques or tau neurofibrillary tangles (Congdon & Sigurdsson, 2018; Perl, 2010), but have failed to result  
70 in effective therapies. Investigations of preventative therapeutics targeting alternative dysfunctional  
71 mechanisms are thus warranted (Crous-Bou et al., 2017). A promising target is the hyperactive signaling  
72 of the Ca<sup>2+</sup>/calmodulin-dependent protein phosphatase calcineurin and its substrate transcription  
73 factor, the nuclear factor of activated T-cells (NFAT). A $\beta$  plaque aggregation is linked to aberrant  
74 calcineurin/NFAT hyperactivity within neurons and astrocytes, leading to neuroinflammation, Ca<sup>2+</sup>  
75 dysregulation, synaptic dysfunction, and excitotoxicity (Norris et al., 2005; Kuchibhotla et al., 2008;  
76 Reese & Tagliatela, 2010). This hyperactivity is associated with cognitive dysfunction in transgenic AD  
77 models (Sompol et al., 2017) and in early AD patient tissue (Abdul et al., 2009, 2011). Calcineurin  
78 inhibition ameliorates these effects in transgenic mouse models of AD (Tagliatela et al., 2009; Stallings  
79 et al., 2023), and was previously linked to a profound reduction in dementia incidence among solid  
80 organ transplant patients maintained on calcineurin inhibitors (Tagliatela et al., 2015). Our group  
81 recently showed that a low dose of the FDA-approved calcineurin inhibitor (CNI) tacrolimus protected  
82 against age-related microstructural gray matter changes within the hippocampus, parahippocampal  
83 gyrus, and prefrontal cortex of middle-aged beagles compared to placebo after one year (Radhakrishnan  
84 et al., 2021). This offers promising evidence for the potential of tacrolimus repurposed as a preventative  
85 treatment of AD.

86 Postmortem evaluations in beagles describe typical age-related characteristics across the canine  
87 lifespan in great detail (Vite & Head, 2014), but *in vivo* characterizations are limited. Of the available  
88 cross-sectional MRI studies in beagles, findings largely align with postmortem evidence of ventricular  
89 widening (González-Soriano et al., 2001; Kimotsuki et al., 2005), early vulnerability of the frontal lobe,  
90 (Tapp et al., 2004) and later vulnerability of the hippocampus to neuron loss (Tapp et al., 2004).  
91 However, individual differences among aging canines, even within the same breed, parallel the  
92 structural heterogeneity of the aging human brain, adding ambiguity to cross-sectional examinations  
93 (Cotman & Head, 2008). Furthermore, age and cohort effects pose additional challenges to  
94 interpretations of findings (O'Brien, 2017).

95 Longitudinal studies are fundamentally immune to such effects and allow for direct assessments  
96 of individual trends over time. While prior MRI studies in aging canines qualitatively assessed  
97 neuroanatomy (Gross et al., 2010) or employed visually guided methods for large-scale brain aging  
98 characteristics (Su et al., 2005), visual inspection alone falls short in detecting subtle alterations during  
99 aging or assessing long-term interventional effects often measured at the submillimeter level in  
100 histological evaluations.

101 Innovative software for analyzing human neuroimaging data have been successfully applied to  
102 just a handful of canine studies but have regularly required some user intervention for standard  
103 preprocessing procedures including brain extraction (Milne et al., 2016), or for delineating brain regions  
104 (Tapp et al., 2004), which can be time-consuming and prone to user error when manually performed.  
105 Hence, an analytical framework for applying automated and standardized methods for reliable  
106 longitudinal analysis for canine imaging data is necessary for enhancing reproducibility and translating  
107 neuroimaging biomarker endpoints to clinical trial outcomes.

108 To this end, we leveraged advanced, open-source image analysis tools to evaluate structural  
109 alterations in a prevention study in healthy middle-aged beagles undergoing chronic CN/NFAT inhibitor  
110 treatment and behavioral enrichment. Regional volume changes were assessed using atlas-based  
111 volumetry as well as deformation-based morphometry (DBM) from high-resolution T1-weighted imaging  
112 collected annually for three years. We hypothesized that aging would be associated with brain region  
113 specific losses in volume that may be protected by a combination treatment approach with behavioral  
114 enrichment and CN or NFAT inhibitor treatment.

115

## 116 **Materials and Methods**

### 117 ***Experimental Design***

#### 118 ***Animals***

119 The study began with forty-five purpose-bred intact adult beagles assessed for general health  
120 status and cognition, as previously described (Christie et al., 2008; Head et al., 1998; Milgram et al.,  
121 1999; Studzinski et al., 2006; Tapp et al., 2003). The final sample included 43 dogs (36 females, 7 males)  
122 ranging from 5 to 8.7 years old. The dogs were then divided into three groups. One group was treated  
123 with a placebo (n=14) while two groups were treated with a chronic low dose of the FDA-approved CNI  
124 tacrolimus (n=15) or the NFAT-inhibiting small chemical compound Q134R (Hackler et al., 2019; Sompol  
125 et al., 2021) (n=14) as part of a longitudinal preclinical study investigating their potential for preventing  
126 AD-related pathology when treated in middle age (Fig. 1). Tacrolimus was given at 0.075 mg/kg (2X daily,  
127 P.O.). Dosage for Q134R was increased after the first year of treatment from 4 mg (2X daily, P.O.) to 8  
128 mg (2X daily, P.O.) for years two and three. Two dogs required euthanasia prior to reaching the third  
129 year of MRI scanning (T3) after their spontaneous development of health conditions unrelated to  
130 treatment that were unable to be sufficiently managed with medical intervention (Table 1).

131 Blood samples were taken every six months to monitor overall health and potential adverse  
132 effects via assessments of blood urea nitrogen, creatine, and phosphorous levels since tacrolimus can

133 cause nephrotoxicity in solid organ transplant patients at higher doses (Randhawa et al., 1997). All  
134 institutional and national guidelines for the care and use of laboratory animals were followed.

135

### 136 ***Behavioral enrichment***

137 The behavioral enrichment paradigm consisted of daily exercise, socialization, cognitive testing,  
138 rotating toys, and social compatible group indoor/outdoor free play. Free play was provided for thirty  
139 minutes and in male-only or female-only groups. Sex-matched dogs were pair-housed in the mornings  
140 and split into their individual kennels in the afternoon prior to feeding. Six sets of two play objects were  
141 rotated through each kennel at weekly intervals. Furthermore, dogs were trained and tested on a  
142 battery of neurocognitive tests designed to capture age-related decline across several cognitive  
143 domains. Briefly, the tasks included spatial learning and memory tasks, landmark discrimination, oddity  
144 discrimination, size discrimination, black/white discrimination, as well as reversal learning. Detailed  
145 descriptions of these tasks are described by Davis et al (Davis et al., 2017). The dogs were tested at  
146 baseline prior to receiving treatment and continuously trained and tested on these tasks 5 days/week  
147 (20-40 min depending on the task) throughout the entirety of the study.

148

### 149 ***Neuroimaging***

150

### 151 **IMAGING DATA ACQUISITION**

152 Imaging data were collected at the Magnetic Resonance Imaging and Spectroscopy Center  
153 (MRISC) at the University of Kentucky in Lexington, KY, USA. Animals were fasted overnight and placed  
154 under general anesthesia using propofol (4-8 mg/kg, i.v., by slow injection to effect). Following induction  
155 and orotracheal intubation, anesthesia was maintained with 1-4% isoflurane delivered in 100% O<sub>2</sub>  
156 during magnetic resonance imaging (MRI) scanning. As part of the standard protocol, dogs were also  
157 premedicated with 0.4 mg/kg of Meloxicam as a prophylaxis for CSF collection-induced soft-tissue injury  
158 and headache/nausea. All CSF collections were completed post-MRI. A 3T MRI scanner (Siemens Prisma  
159 Fit) with a 15-channel transmit-receive knee coil was used to scan the canine brain across 4 time points:  
160 at baseline before treatment with placebo, tacrolimus or Q134R (T0), and annually for three years (T1-  
161 T3). For structural imaging, a high-resolution T1-weighted image was collected using a magnetization-  
162 prepared rapid gradient-echo (MPRAGE) sequence (repetition time (TR)=2530 ms; echo time (TE) = 2.49  
163 ms; flip angle = 7°; matrix size = 0.4 x 0.4 x 0.7 mm; averages = 1; average acquisition time = 10 min, 30 s;  
164 voxel size 0.352x0.352mm, slice thickness 0.7mm).

165

### 166 **IMAGE PROCESSING**

167 The T1-weighted images were first visually inspected for quality control. No obvious adverse  
168 effects of treatment on brain structure were identified for any dogs. Minor ghosting artifacts that did  
169 not overlap with the brain were edited out from the 3D images of two dogs to overcome faulty  
170 registration during image preprocessing. Next, all images were processed using the Advanced

171 Normalization Tools (ANTs) software (version 2.3.1). ANTs has an extensive track-record of robust  
172 performance in lifespan analyses of brain morphology (Tustison et al., 2014) and has been recently  
173 implemented in canine neuroimaging studies for the development of *in vivo* and *ex vivo* group templates  
174 and digital atlases (Czeibert et al., 2019; Datta et al., 2012; Johnson et al., 2020). The high-resolution  
175 group template developed for an earlier report on the tacrolimus-treated and placebo-treated dogs was  
176 used in the present study (Radhakrishnan et al., 2021). For atlas-based ROI analyses, we used a recently  
177 developed high-resolution stereotaxic canine brain atlas with detailed parcellations (Johnson et al.,  
178 2020) and created a simplified version by grouping cortical parcellations by their respective gyri. This  
179 simplified atlas, hereby referred to as the “Johnson atlas,” was registered to the group template space  
180 using the affine+SyN algorithm for diffeomorphic image registration. Finally, CSF posteriors were  
181 obtained from processing the group template through the ANTs cortical thickness pipeline and were  
182 added to the CSF segmentation map by Johnson et al. (Johnson et al., 2020) which was then binarized  
183 and smoothed to create a more detailed CSF prior probability map that can better resolve CSF  
184 compartments within narrow sulci.

185 Individual image processing was then performed using a longitudinal image analysis pipeline  
186 newly available within ANTs that has demonstrated superior performance in humans for detecting  
187 disease-related structural alterations from serial neuroimaging (Tustison et al., 2019) and interventional  
188 effects in clinical trials (Song et al., 2022). Here, minor customizations were made to the pipeline to  
189 account for canine brain size and voxel dimensions. An important feature of this pipeline is the creation  
190 of an unbiased single-subject template (SST) used as an intermediate reference space between the  
191 group template and time point images for reducing registration errors and optimizing sensitivity to  
192 longitudinal volume changes (Fig. 1). In the pipeline, each dog’s SST was first generated from its set of  
193 T1-weighted images that underwent preprocessing including N4 bias-field correction (Tustison et al.,  
194 2010), brain extraction, and probabilistic tissue segmentation via Atropos (Avants et al., 2011) with  
195 reference to the group template, resulting in prior probability maps in the space of the SST as well as  
196 non-linear SST to group template warps. Each time point image was then rigidly aligned to the SST and  
197 denoised prior to undergoing the same preprocessing steps as the SST while treating the SST as the  
198 reference template, resulting in tissue segmentation maps and warps to the SST for each time point  
199 image.

200

## 201 **ROI-BASED VOLUMETRY**

202 To obtain regional volume measures at each time point, the Johnson atlas was registered to the  
203 processed time point images by applying the warps generated from combining the template to SST and  
204 SST to time point warps. The volume of each region was calculated in each dog’s native time point space  
205 as the sum of all voxels within each atlas parcellation with CSF voxels subtracted converted to cubic  
206 millimeters. The left and right ROI volumes were adjusted by the log-Jacobian determinant of the linear  
207 SST to group template transformation of each animal, a scalar value associated with approximate  
208 intracranial volume (ICV) (Buckner et al., 2004) and z-transformed with respect to each ROI’s mean  
209 baseline volume. We did not observe any significant differences between bilateral ROIs at baseline so  
210 mean bilateral volumes were calculated for subsequent analysis.

211 Several cortical ROIs and the cerebellum were excluded from further analysis due to erroneous  
212 tissue segmentations at brain versus non-brain boundaries for several dogs at various time points.  
213 Brainstem and claustrum ROIs defined within the original Johnson atlas were not included in the  
214 analysis. A final total of 24 bilateral ROIs were examined that included cortical structures from frontal,  
215 sensory-motor, cingulate, occipital, parietal lobar areas as well as three subcortical structures:  
216 amygdala, caudate nucleus, and hippocampus (Table 2).

217

## 218 **DEFORMATION-BASED MORPHOMETRY**

219 As a complimentary volumetric analysis, we performed deformation-based morphometry (DBM)  
220 for a more granular, voxel-based assessment of volume changes. Briefly, maps of the non-linear warps  
221 generated from voxel-wise registration of each image to a reference image in the same coordinate  
222 space (e.g., the time point image moving to the SST) can be converted to a log-Jacobian determinant  
223 map which represents the amount of expanding or contracting of each voxel during the registration.  
224 When registering to a common template space, the log-Jacobians can be considered a voxel-based  
225 summary measure of volume that can be compared across individuals (Ashburner et al., 1998). Here, we  
226 combined the warps generated from the time point to the SST registration and SST to the group  
227 template registration during preprocessing. Creating “DBM maps” by this method, these maps are set in  
228 the group template space that capture each dog’s longitudinal changes with respect to its SST as well as  
229 cross-sectional differences with respect to the group template. Each DBM map was resampled to a  
230 0.5mm isotropic resolution and was slightly eroded by two voxels to exclude problematic edge voxels  
231 that were found to include CSF, pia, or dura in several dogs’ native space (Fig. 1).

232

## 233 ***Statistical analysis***

234

## 235 **ROI VOLUMETRY**

236 First, for an initial evaluation of general atrophy rates regardless of treatment group, we  
237 calculated simple ROI volume slopes over time for each dog from bivariate ordinary least squares  
238 regressions. We then used a non-parametric rank analysis for evaluating differences between regional  
239 atrophy rates using the Friedman test. We performed post-hoc pairwise comparisons of rank-sum  
240 differences as well as one-sample t tests against zero on each set of ROI slopes and adjusted for multiple  
241 comparisons using Dunn’s post-hoc test from the SciPy library in Python.

242 Next, we conducted separate multivariate linear mixed effects (LME) analyses per ROI. LME  
243 models can flexibly account for incomplete data, dependency within repeated within-subjects  
244 measurements, and hierarchically structured data, which can improve the reproducibility of longitudinal  
245 studies (Yu, Guindani, et al., 2022). To predict ROI volume, we assigned treatment group, baseline age,  
246 years elapsed since the initial baseline scan (“time”), and a time by treatment interaction term as fixed  
247 effects, and a random intercept was assigned at the level of individual dogs (i.e. random effect of  
248 subject). The p-values for the LME parameter estimates from each ROI analysis were adjusted for  
249 multiple comparisons using the Holm-Sidak method for a family-wise error rate of 5%.

250 Lastly, we used an all-ROI-inclusive LME model by adding “region” as a predictor variable to  
251 evaluate differential patterns of volume changes in a single model using the hippocampus as the  
252 reference level. The region with the least decline observed from the two prior analyses was used as the  
253 reference ROI in the model. Since the per-region LME models did not show reliable evidence for  
254 treatment by time interactions (Fig. 4), the treatment predictor was excluded from this LME analysis to  
255 evaluate sample-wide trends in volume changes regardless of treatment group. Thus, the fixed effects  
256 for this model included region, time, z-transformed baseline age, a time by region interaction term, and  
257 a random intercept was again assigned per dog. Here, the estimates for baseline age and time attributed  
258 to the reference region, and the estimates for each time by region interaction are thus conditional on  
259 the estimated effect of time. Diagnostic model fit evaluations using the Akaike Information Criterion  
260 (AIC) and the Bayesian Information Criterion (BIC) indicated that a model excluding treatment was  
261 indeed preferred over a model that included interactions with treatment.

262

## 263 **DBM ANALYSIS**

264 We conducted a brain-wide linear mixed effects analysis of voxel-wise volume change on the  
265 DBM maps using the 3dLMER package in the Analysis of Functional NeuroImages (AFNI) software suite  
266 (Chen et al., 2013). Here, treatment group, baseline age, time, and a time by treatment interaction term  
267 were assigned as fixed effects, and a random effect was assigned per dog for predicting the log-Jacobian  
268 determinant (i.e., volume) per voxel. Baseline age values were centered on the mean baseline age of 6.7  
269 years (age – mean age) and time was centered on baseline year (time=0). Minimum cluster size  
270 thresholds for the Z-statistical maps of each main effect, interaction, and for treatment contrasts over  
271 time (tacrolimus over Time vs. Placebo over Time, Q134R over Time vs. Placebo over Time), correcting  
272 for multiple comparisons, were empirically determined from 100 Monte Carlo simulations in 3dLMER.  
273 Baseline age and treatment were permuted across subjects and time was permuted within subjects.  
274 Each critical cluster size was determined from the 5% probability of the largest resulting false-positive  
275 clusters generated using AFNI’s 3dClusterize with a voxel-wise threshold of  $p=0.0001$ .

276

## 277 **Code availability**

278 Code for data processing and analysis is available at <https://github.com/StarkLabUCI/canine-long-sMRI>.

279

## 280 **Results**

### 281 ***Regional selectivity of volume losses, hippocampal volume increases***

282 First, rank analyses of the dog-specific slopes of volume over time revealed consistent patterns  
283 of cortical volume loss among 17 cortical ROIs (Fig. 2a,b, Table 2). All frontal lobe ROIs, including the  
284 pregenual, proreus, and orbital gyri, were ranked highest for exhibiting the most rapid rates of volume  
285 loss (orbital gyrus: median slope (z)=-0.17, median rank=5 out of 24; gyrus proreus: median slope=-0.21,  
286 median rank=5; pregenual gyrus: median slope=-0.15, median rank=6) (Fig. 3) and declined significantly  
287 faster than ten other regions (Fig. 2b). Furthermore, the posterior compositus and sylvian gyri within the

288 temporal lobe ranked next highest for rapid volume loss (posterior compositus gyrus: median slope=-  
289 0.18, median rank=6; sylvian gyrus: median slope=-0.14, median rank=8). There was no apparent  
290 evidence of volume loss from the simple volume slopes of the genualis, suprasylvian, parietal coronal,  
291 and entolateral gyri, or from the amygdala (Table 4). Most notably and contrary to typical brain aging in  
292 canines (Tapp et al., 2004; Su et al., 2005; Kimotsuki et al., 2005), the hippocampus showed strong  
293 evidence of unique volumetric increases over time (median slope=0.16, median rank=24) and the  
294 caudate nucleus also showed evidence for a mild volumetric increase (median slope=0.06, median  
295 rank=22) (Fig. 2a,b, Fig. 3, Table 4). The remaining regions in the cingulate, sensory-motor, occipital, and  
296 parietal lobes also showed volume loss but to a lesser extent (Fig 2a, Table 4).

297

298

299 Next, we employed separate multivariate LME models per ROI to test for longitudinal effects of  
300 treatment and baseline age on volume losses as a function of time. We did not observe any significant  
301 time-by-treatment interactions for tacrolimus or Q134R for any ROIs after adjusting for multiple  
302 comparisons. The regions that showed a significant main effect of time on volume loss were largely  
303 consistent with the regions found to decline in the above simple slope analyses. However, we found that  
304 the LME models for the ectosylvian, parietal marginal, recurrens, and proreus gyri, and the caudate  
305 nucleus did not show sufficient evidence of any volume changes over time (Fig. 4). A strong increase in  
306 hippocampal volume over time across all groups was also evident by LME analysis ( $\beta=0.154$ ,  $SE=0.034$ ,  
307 adjusted  $p<0.001$ ,  $CI[0.088, 0.220]$ ).

308 The noteworthy increases in hippocampal volume across all groups motivated the use of the  
309 larger, all-ROI-inclusive LME analysis to directly contrast its rate of decline to that of each ROI in a single  
310 model. Here, the parameter estimates for each ROI are conditional upon the main effects of time and  
311 age, with the volume of the hippocampus as the reference region (Fig. 5a). Treatment group was  
312 excluded from this model due to the lack of evidence for treatment effects in every per-region LME  
313 analysis. We found volume increases in hippocampal volume over time as we observed in our prior  
314 analyses ( $\beta=0.181$ ,  $SE=0.048$ ,  $p<0.001$ ,  $CI[0.087, 0.275]$ ), which equates to a 1.74% average annual  
315 increase in volume. Critically, every time-by-region interaction apart from the caudate nucleus showed  
316 distinct rates of volume decline relative to the hippocampus, underscoring the unique trajectory of  
317 hippocampal volume changes over the three years. Furthermore, the differential pattern of volume  
318 decline across the other ROIs were highly consistent with the simple slope analysis, specifically the  
319 accelerated volume decline of frontal pregenual, proreus, and orbital gyri and temporal posterior  
320 compositus gyrus (Fig. 5a,b). The full set of parameter estimates for this model can be found in Table 5.

321

### 322 ***Characterizing whole-brain spatiotemporal patterns of volume changes using DBM***

323 Atlas-based approaches to assessing volumetry have their clear merits but run the risk of  
324 missing patterns or effects that do not correlate well with region boundaries, which motivated the use  
325 of whole-brain DBM. Thus, we conducted a voxel-wise linear mixed effects analysis of the log-Jacobians  
326 or “DBM maps” that were generated from spatial registrations of the time point images to the SST and

327 group templates. We used a strict voxel-wise threshold of  $p=0.0001$  to identify clusters of the most  
328 extreme volume changes predicted by time, baseline age, and treatment by time interactions.

329 Consistent with the ROI-based LME analyses, post-hoc linear contrasts examining differences  
330 from placebo for time by treatment interactions (tacrolimus-placebo minimum cluster size threshold =  
331  $29 \text{ mm}^3$ ; Q134R-placebo minimum cluster size threshold =  $15 \text{ mm}^3$ ) did not yield any significant clusters  
332 of treatment-related effects on volume change by tacrolimus or by Q134R (data not shown).

333 Next, we wanted to examine cross-sectional aging effects on regional volume in the brain  
334 independent of longitudinal treatment effects. A cluster analysis of the log-Jacobians revealed five  
335 clusters for the main effect of age on volume decline ( $\log\text{-Jacobian}<0$ ) on all treatment groups with time  
336 fixed at baseline (minimum cluster-size threshold =  $25 \text{ mm}^3$ ). We found evidence of focal volume loss  
337 with every unit increase in age that was mainly posteriorly localized in the brain (Fig. 6a-d). The largest  
338 cluster of reduced volumes was found in the occipital marginal gyrus, medial occipital gyrus, and  
339 posterior cingulate gyrus in the left hemisphere ( $53 \text{ mm}^3$ ) (Fig. 6c), and the next largest cluster  
340 encompassed only the occipital marginal gyrus and the medial occipital gyrus in the right hemisphere  
341 ( $47 \text{ mm}^3$ ; Fig. 6c). A smaller cluster spanning the occipital and temporal lobes was found within the left  
342 suprasylvian and ectosylvian gyri ( $35 \text{ mm}^3$ ; Fig. 6b) and similar-sized cluster was found within the  
343 interthalamic adhesion ( $19 \text{ mm}^3$ ; Fig. 6d). Lastly, a cluster within the left occipital lobe spanning the left  
344 inferior medial occipital gyrus and pararecurrans ( $16 \text{ mm}^3$ ) had the most extreme age-related volume  
345 loss at baseline (Fig. 6a).

346 Next, to assess the volumetric changes over three years in the study which included behavioral  
347 enrichment across all groups, we performed a cluster analysis for the main effect of time from the DBM  
348 maps (minimum cluster-size threshold= $10 \text{ mm}^3$ ) (Fig. 7). Our DBM findings corroborated our ROI-based  
349 results where cortical shrinkage ( $\log\text{-Jacobian}<0$ ) was the most prominent in frontal and temporal lobes.  
350 Furthermore, the greater spatial precision of this voxel-based volumetric estimation identified hotspots  
351 of volume loss within the posterior cingulate gyrus and the suprasylvian gyrus. The segmentation-  
352 agnostic DBM maps also allowed us to assess areas not defined by the Johnson atlas or ROIs that were  
353 previously excluded due to segmentation issues. We found rapid annual volume loss within the gyrus  
354 subproneus of the frontal lobe, the precruciate, pre- and postcentral gyri of the sensory-motor lobe, as  
355 well as significant volume loss within the genu, body, and splenium of the corpus callosum, and within  
356 midbrain and brainstem areas. Cerebellum clusters not shown.

357  
358 Conversely, areas of significant expansion ( $\log\text{-Jacobian}>0$ ) were observed over the lateral  
359 ventricles indicating ventricular widening, consistent with typical canine aging (Gunde et al., 2020; Su et  
360 al., 2005) (Fig. 7). The hippocampus had significant expansion along most of the dorsal hippocampus,  
361 but the ventral hippocampus was largely unchanged (Fig. 8). Furthermore, we found that the third  
362 ventricle immediately adjacent to dorsal hippocampus showed extreme volume loss which is consistent  
363 with dorsal hippocampal volume expansion. Lastly, we observed unexpected expansion across occipital  
364 and frontal white matter areas consistent with experience-dependent white matter plasticity (Mendez  
365 Colmenares et al., 2021) (Fig. 7).

366

## 367 Discussion

368 In this study, we investigated cortical and subcortical volume changes in aging beagles, a natural  
369 model of AD (Cotman & Head, 2008; Vite & Head, 2014), undergoing long-term behavioral enrichment  
370 and tacrolimus, Q134R, or placebo treatment beginning in middle age. Our main goal was to explore the  
371 spatiotemporal patterns of brain atrophy in normal canine aging and assess the potential  
372 neuroprotective effects of CN/NFAT inhibitor treatment on brain volume. Using segmentation-based ROI  
373 volumetry and whole-brain, voxel-based DBM, we uncovered striking and unexpected evidence of  
374 increased bilateral hippocampal volume in all three groups across three years.

375 Our ROI-based evaluations showed that total hippocampal volume increased at an average rate  
376 of about 1.74% per year across treatment groups, contrasting with the age-related hippocampal volume  
377 decline observed in previous cross-sectional neuroimaging studies in laboratory beagles (Tapp et al.,  
378 2004). We did not observe any relationships between age and hippocampal volume at baseline prior to  
379 the behavioral enrichment protocol (Fig. 9), suggesting that the hippocampal volume increases were  
380 likely not a feature of typical hippocampal maturation in beagles. Instead, we argue that these increases  
381 may be attributed to the high levels of behavioral enrichment in the present study that included social  
382 interaction, exploration, physical exercise, and sensory stimulation, all of which are known to induce a  
383 number of neurobiological changes. Previous studies showed behaviorally-enhanced adult neurogenesis  
384 in canines within the hilus of the dentate gyrus (DG) following behavioral enrichment (Siwak-Tapp et al.,  
385 2008) and a dorsal-ventral gradient in neurogenic potential in the canine hippocampus (Bekiari et al.,  
386 2020). Although in the present study our DBM results showed volumetric increases that were mainly  
387 localized to dorsal hippocampus, whether these changes were primarily attributed to hippocampal  
388 neurogenesis is limited to speculation given the lack of a non-enriched control group in this study.  
389 Furthermore, other exercise-related angiogenic mechanisms such as vascular plasticity and increased  
390 cerebral blood volume may drive up hippocampal volume as well (Kim et al., 2021), which has been  
391 observed with high-resolution MRI in human adult exercise intervention studies (Maass et al., 2015).  
392 Whether angiogenesis and neurogenesis are interdependent mechanisms at play in the hippocampus, or  
393 in other regions that possibly undergo adult neurogenesis such as the hypothalamus (Fowler et al.,  
394 2008), remains to be explored. A key aim of our histological analyses at the conclusion of the study will  
395 be to examine altered molecular and cellular signatures of neurogenesis related to CN/NFAT treatment  
396 that will be valuable to the growing body of research targeting neurogenic mechanisms in AD (Babcock  
397 et al., 2021).

398 We did not identify treatment-related modulation to hippocampal volume or to any other brain  
399 region by CN inhibition with tacrolimus nor by NFAT inhibition with Q134R. However, our group has  
400 previously shown that multi-shell DWI, an imaging technique sensitive to microstructural gray and white  
401 matter changes (Alexander et al., 2007; Afzali et al., 2021; Radhakrishnan et al., 2022), showed age-  
402 related microstructural changes within the hippocampus, parahippocampal gyrus, and prefrontal cortex  
403 in placebo-treated dogs that were slower in tacrolimus-treated dogs after just one year (Radhakrishnan  
404 et al., 2021). Our negative finding with the current volumetric analysis is not surprising considering that  
405 tacrolimus, Q134R and other peptide-based strategies targeting CN/NFAT-related signaling are known to  
406 affect cytoarchitectural and biochemical features including synaptic plasticity, neuroinflammation, and  
407 glutamate regulation (Dineley et al., 2007; Furman et al., 2012; Hudry et al., 2012; Sompol et al., 2017)  
408 that macrostructural measurements derived from T1-weighted imaging cannot detect. Furthermore, the

409 majority of the dogs in this study had not yet reached the typical age where the effects of increasing A $\beta$   
410 burden such as oxidative stress, neurotoxicity, and neuronal loss become more prevalent, which begins  
411 around nine years old for beagles (developmentally similar to 60-year-old humans). (Cotman & Head,  
412 2008). Thus, the final two MRI sessions for the dogs collected at mean ages of 10.5 and 11.5 years will  
413 offer greater insights into whether chronic CN/NFAT inhibition ameliorates impairments related to A $\beta$   
414 burden and/or ultimately slows the trajectory of age-related cortical and subcortical atrophy.  
415 Importantly, the lack of treatment effects on brain structure and age-associated volumetric losses  
416 suggests that although there may be no benefits currently on this outcome measure, long-term  
417 treatment with tacrolimus or Q134R does not appear to accelerate brain atrophy, which was recently  
418 found to be prevalent across numerous clinical trials for anti-A $\beta$  therapies (Alves et al., 2023). However,  
419 we will continue to comprehensively monitor the safety and tolerability of these compounds following  
420 chronic administration in the aging beagles from neuroimaging and other standard safety measures.

421         Across all treatment groups, we observed volume losses across numerous cortical areas as well  
422 as ventricular enlargement, all consistent with prior reports of canine neuroimaging findings (Su et al.,  
423 1998; Kimotsuki et al., 2005). Importantly, our observations recapitulate the differential patterns of  
424 volume decline previously observed in aging beagles such as accelerated atrophy of the frontal lobe  
425 (Tapp et al., 2006). The prefrontal cortex is an early site of A $\beta$  accumulation in both aging humans and  
426 canines (Head et al., 2000), which makes structural changes to this region an informative neuroimaging  
427 biomarker of potential AD-related neurodegeneration. Conversely, its preservation can be used as a  
428 biomarker of interest to distinguish effects of CNI or NFAT inhibitor treatment at the conclusion of the  
429 study. Interestingly, while a prior cross-sectional study by Tapp et al. (Tapp et al., 2004) suggests frontal  
430 lobe atrophy occurs around ten years of age, their work did not include dogs between 7 to 9 years. Our  
431 longitudinal findings address this gap and suggest that the onset of frontal lobe volume decline occurs  
432 early during middle age, beginning as early as 5 years old in some of the dogs in the present study.  
433 Future work in comparison to non-enriched animals can shed light on whether the rate of frontal lobe  
434 volume loss may have been attenuated by enrichment.

435         The greater spatial sensitivity of the voxel-based DBM analysis revealed focal areas of significant  
436 age-related volume decline at baseline within the cingulate, occipital, and temporal lobes. Among these  
437 regions included the posterior cingulate gyrus, a region associated with early A $\beta$  accumulation  
438 (Palmqvist et al., 2017), hypometabolism (Minoshima et al., 1997), synapse loss (Scheff et al., 2015;  
439 Scheff & Price, 2001), disrupted functional connectivity (Berron et al., 2020), and atrophy in the earliest  
440 phases of AD (Pengas et al., 2010). Prior work in beagles at 14 years old report extensive A $\beta$  plaque  
441 aggregates in the cingulate cortex (Pop et al., 2012), but the time course of neurodegeneration in this  
442 region that may precede A $\beta$  accumulation has not been characterized in beagles during middle age. Our  
443 findings provide the first *in vivo* evidence to our knowledge of posterior cingulate atrophy occurring as  
444 early as middle age that parallels human posterior cingulate atrophy and precedes frontal lobe atrophy  
445 in canines.

446         Furthermore, we identified novel volume preservation of the caudate nucleus. Interestingly, our  
447 baseline evaluation of cross-sectional volumes with respect to age showed a trend in caudate nucleus  
448 volume decline ( Fig. 9), suggesting that exposure to our behavioral enrichment protocol may have  
449 contributed to its attenuation in volume changes across all groups (Fig. 5a,b). The caudate nucleus is  
450 part of an extensive prefrontal-striatal network that is involved in numerous functions, including

451 coordination and motor planning (Fuster, 2002), and its volume steadily declines throughout human  
452 adulthood (Raz et al., 2003). In beagles, the caudate nucleus exhibits reduced glucose metabolism by  
453 middle age (London et al., 1983), and along with the frontal cortex, is at risk for developing lesions in the  
454 form of lacunar infarcts or cysts (Su et al., 2005). More work is necessary to understand whether the  
455 preserved volumes of the caudate nucleus may be a result of daily exercise and training on numerous  
456 reward-based visuomotor tasks, similar to preservations previously observed in older human adults  
457 under long-term motor coordination training (Niemann et al., 2014).

458 Additionally, our voxel-wise DBM analysis also uncovered unexpected areas of white matter  
459 expansion among areas with well-documented white matter degradation in middle aged humans (Raz et  
460 al., 2010). Long-term behavioral interventions such as training on a new visuomotor skill (Scholz et al.,  
461 2009), aerobic exercise (Mendez Colmenares et al., 2021), and memory training (De Lange et al., 2018)  
462 can induce white matter enhancements in human adults. DWI assessments are currently being  
463 performed in the dogs to further characterize these potential enrichment-associated alterations in both  
464 gray and white matter microstructure in greater detail.

465 Our ROI-based analyses were important descriptive analyses that can enhance statistical power  
466 by limiting the number of tests but can be prone to providing an incomplete picture by potentially  
467 artificially segregating the brain. Here, the problem was exacerbated by having several ROIs excluded on  
468 the basis of problematic segmentations during image preprocessing. A previous study comparing  
469 manual versus automated methods for brain extraction found that manual masking was still superior  
470 (Milne et al., 2016), indicating that more work is necessary for refining these image preprocessing  
471 procedures for canine data. Recently developed tools have leveraged deep learning for improving the  
472 accuracy of brain extraction performance (Tustison et al., 2021; Yu, Han, et al., 2022) but have been  
473 trained on human images and have yet to be adapted for canines. However, our novel application of  
474 DBM in the canine offers a more agnostic view to volumetric changes with greater spatial precision and  
475 was a valuable complementary approach for assessing morphometric alterations in the present study.

476 We were unable to perform any meaningful evaluations of sex differences because our cohort  
477 of dogs was predominantly female due to the availability of retired female breeders for the study.  
478 However, previous observations of sex differences in canine brain structure (Tapp et al., 2006) as well as  
479 the increasing proportion of women at risk for developing AD dementia over the next four decades  
480 compared to men (Rajan et al., 2021) suggest the need for future investigations to directly assess  
481 potential sex differences in drug efficacy the canine model.

482 Our findings offer novel insights into *in vivo* volume changes that occur during middle age, prior  
483 to the known onset of major A $\beta$  pathology in aging canines. We demonstrate the feasibility of an  
484 automated structural analysis pipeline to assess longitudinal changes in the canine brain at a high level  
485 of detail using state-of-the-art neuroimaging analysis tools designed to detect subtle alterations in brain  
486 morphology. The application of this analytical framework revealed both well-documented and novel  
487 structural alterations to the aging beagle brain and underscore the parallels of cortical and subcortical  
488 longitudinal changes in volume between canines and humans during aging. Our future application of this  
489 analytical framework will be instrumental for examining the utility of our *in vivo* neuroimaging  
490 biomarkers in predicting disease burden and cognitive outcomes under CN/NFAT inhibition. These  
491 findings in a natural model of AD like the beagle offer important contributions to the growing body of

492 research aimed at understanding the role of modifiable lifestyle factors such as exercise, diet, and  
493 cognitive enrichment for reducing the risk of AD (Lista et al., 2015) and suggest that middle age may be a  
494 promising therapeutic window of behavioral intervention.

495

496

## REFERENCES

497

498 Abdul, H. M., Baig, I., Levine, H., Guttmann, R. P., & Norris, C. M. (2011). Proteolysis of calcineurin is  
499 increased in human hippocampus during mild cognitive impairment and is stimulated by  
500 oligomeric Abeta in primary cell culture. *Aging Cell*, *10*(1), 103–113.  
501 <https://doi.org/10.1111/j.1474-9726.2010.00645.x>

502 Abdul, H. M., Sama, M. A., Furman, J. L., Mathis, D. M., Beckett, T. L., Weidner, A. M., Patel, E. S., Baig, I.,  
503 Murphy, M. P., LeVine, H., Kraner, S. D., & Norris, C. M. (2009). Cognitive Decline in Alzheimer's  
504 Disease Is Associated with Selective Changes in Calcineurin/NFAT Signaling. *The Journal of*  
505 *Neuroscience*, *29*(41), 12957–12969. <https://doi.org/10.1523/JNEUROSCI.1064-09.2009>

506 Afzali, M., Pieciak, T., Newman, S., Garyfallidis, E., Özarlan, E., Cheng, H., & Jones, D. K. (2021). The  
507 sensitivity of diffusion MRI to microstructural properties and experimental factors. *Journal of*  
508 *Neuroscience Methods*, *347*, 108951. <https://doi.org/10.1016/j.jneumeth.2020.108951>

509 Alexander, A. L., Lee, J. E., Lazar, M., & Field, A. S. (2007). Diffusion Tensor Imaging of the Brain.  
510 *Neurotherapeutics : The Journal of the American Society for Experimental NeuroTherapeutics*,  
511 *4*(3), 316–329. <https://doi.org/10.1016/j.nurt.2007.05.011>

512 Alves, F., Kalinowski, P., & Ayton, S. (2023). Accelerated Brain Volume Loss Caused by Anti-β-Amyloid  
513 Drugs: A Systematic Review and Meta-analysis. *Neurology*, *100*(20), e2114–e2124.  
514 <https://doi.org/10.1212/WNL.0000000000207156>

515 Araujo, J. A., Segarra, S., Mendes, J., Paradis, A., Brooks, M., Thevarkunnel, S., & Milgram, N. W. (2022).  
516 Sphingolipids and DHA Improve Cognitive Deficits in Aged Beagle Dogs. *Frontiers in Veterinary*  
517 *Science*, *9*, 646451. <https://doi.org/10.3389/fvets.2022.646451>

518 Ashburner, J., Hutton, C., Frackowiak, R., Johnsrude, I., Price, C., & Friston, K. (1998). Identifying global  
519 anatomical differences: Deformation-based morphometry. *Human Brain Mapping*, *6*(5–6), 348–  
520 357. [https://doi.org/10.1002/\(SICI\)1097-0193\(1998\)6:5/6<348::AID-HBM4>3.0.CO;2-P](https://doi.org/10.1002/(SICI)1097-0193(1998)6:5/6<348::AID-HBM4>3.0.CO;2-P)

521 Avants, B. B., Tustison, N. J., Wu, J., Cook, P. A., & Gee, J. C. (2011). An Open Source Multivariate  
522 Framework for n-Tissue Segmentation with Evaluation on Public Data. *Neuroinformatics*, *9*(4),  
523 381–400. <https://doi.org/10.1007/s12021-011-9109-y>

524 Babcock, K. R., Page, J. S., Fallon, J. R., & Webb, A. E. (2021). Adult Hippocampal Neurogenesis in Aging  
525 and Alzheimer's Disease. *Stem Cell Reports*, *16*(4), 681–693.  
526 <https://doi.org/10.1016/j.stemcr.2021.01.019>

- 527 Bekiari, C., Grivas, I., Tsingotjidou, A., & Papadopoulos, G. C. (2020). Adult neurogenesis and gliogenesis  
528 in the dorsal and ventral canine hippocampus. *Journal of Comparative Neurology*, *528*(7), 1216–  
529 1230. <https://doi.org/10.1002/cne.24818>
- 530 Berron, D., van Westen, D., Ossenkoppele, R., Strandberg, O., & Hansson, O. (2020). Medial temporal  
531 lobe connectivity and its associations with cognition in early Alzheimer's disease. *Brain*, *143*(4),  
532 1233–1248. <https://doi.org/10.1093/brain/awaa068>
- 533 Buckner, R. L., Head, D., Parker, J., Fotenos, A. F., Marcus, D., Morris, J. C., & Snyder, A. Z. (2004). A  
534 unified approach for morphometric and functional data analysis in young, old, and demented  
535 adults using automated atlas-based head size normalization: Reliability and validation against  
536 manual measurement of total intracranial volume. *NeuroImage*, *23*(2), 724–738.  
537 <https://doi.org/10.1016/j.neuroimage.2004.06.018>
- 538 Chan, A. D. F., Nippak, P. M. D., Murphey, H., Ikeda-Douglas, C. J., Muggenburg, B., Head, E., Cotman, C.  
539 W., & Milgram, N. W. (2002). Visuospatial impairments in aged canines (*Canis familiaris*): The  
540 role of cognitive-behavioral flexibility. *Behavioral Neuroscience*, *116*(3), 443–454.
- 541 Chen, G., Saad, Z. S., Britton, J. C., Pine, D. S., & Cox, R. W. (2013). Linear mixed-effects modeling  
542 approach to fMRI group analysis. *NeuroImage*, *73*, 176–190.  
543 <https://doi.org/10.1016/j.neuroimage.2013.01.047>
- 544 Christie, L. A., Saunders, R. C., Kowalska, D. M., MacKay, W. A., Head, E., & Cotman, C. W. (2008). Rhinal  
545 and dorsolateral prefrontal cortex lesions produce selective impairments in object and spatial  
546 learning and memory in canines. *J Comp Neurol*, *511*, 257–270.
- 547 Congdon, E. E., & Sigurdsson, E. M. (2018). Tau-targeting therapies for Alzheimer disease. *Nature*  
548 *Reviews. Neurology*, *14*(7), 399–415. <https://doi.org/10.1038/s41582-018-0013-z>
- 549 Cotman, C. W., & Head, E. (2008). The Canine (Dog) Model of Human Aging and Disease: Dietary,  
550 Environmental and Immunotherapy Approaches. *Journal of Alzheimer's Disease*, *15*(4), 685–707.  
551 <https://doi.org/10.3233/JAD-2008-15413>
- 552 Crous-Bou, M., Minguillón, C., Gramunt, N., & Molinuevo, J. L. (2017). Alzheimer's disease prevention:  
553 From risk factors to early intervention. *Alzheimer's Research & Therapy*, *9*(1), 71.  
554 <https://doi.org/10.1186/s13195-017-0297-z>
- 555 Czeibert, K., Andics, A., Petneházy, Ö., & Kubinyi, E. (2019). A detailed canine brain label map for  
556 neuroimaging analysis. *Biologia Futura*, *70*(2), 112–120. <https://doi.org/10.1556/019.70.2019.14>
- 557 Datta, R., Lee, J., Duda, J., Avants, B. B., Vite, C. H., Tseng, B., Gee, J. C., Aguirre, G. D., & Aguirre, G. K.  
558 (2012). A Digital Atlas of the Dog Brain. *PLOS ONE*, *7*(12), e52140.  
559 <https://doi.org/10.1371/journal.pone.0052140>
- 560 Davis, P. R., Giannini, G., Rudolph, K., Calloway, N., Royer, C. M., Beckett, T. L., Murphy, M. P., Bresch, F.,  
561 Pagani, D., Platt, T., Wang, X., Donovan, A. S., Sudduth, T. L., Lou, W., Abner, E., Kryscio, R.,  
562 Wilcock, D. M., Barrett, E. G., & Head, E. (2017). A $\beta$  vaccination in combination with behavioral  
563 enrichment in aged beagles: Effects on cognition, A $\beta$ , and microhemorrhages. *Neurobiology of*  
564 *Aging*, *49*, 86–99. <https://doi.org/10.1016/j.neurobiolaging.2016.09.007>

- 565 De Lange, A.-M. G., Bråthen, A. C. S., Rohani, D. A., Fjell, A. M., & Walhovd, K. B. (2018). The Temporal  
566 Dynamics of Brain Plasticity in Aging. *Cerebral Cortex*, 28(5), 1857–1865.  
567 <https://doi.org/10.1093/cercor/bhy003>
- 568 Dineley, K. T., Hogan, D., Zhang, W.-R., & Tagliabue, G. (2007). Acute inhibition of calcineurin restores  
569 associative learning and memory in Tg2576 APP transgenic mice. *Neurobiology of Learning and*  
570 *Memory*, 88(2), 217–224. <https://doi.org/10.1016/j.nlm.2007.03.010>
- 571 Fowler, C. D., Liu, Y., & Wang, Z. (2008). ESTROGEN AND ADULT NEUROGENESIS IN THE AMYGDALA AND  
572 HYPOTHALAMUS. *Brain Research Reviews*, 57(2), 342–351.  
573 <https://doi.org/10.1016/j.brainresrev.2007.06.011>
- 574 Furman, J. L., Sama, D. M., Gant, J. C., Beckett, T. L., Murphy, M. P., Bachstetter, A. D., Van Eldik, L. J., &  
575 Norris, C. M. (2012). Targeting Astrocytes Ameliorates Neurologic Changes in a Mouse Model of  
576 Alzheimer’s Disease. *The Journal of Neuroscience*, 32(46), 16129–16140.  
577 <https://doi.org/10.1523/JNEUROSCI.2323-12.2012>
- 578 Fuster, J. M. (2002). Frontal lobe and cognitive development. *Journal of Neurocytology*, 31(3), 373–385.  
579 <https://doi.org/10.1023/A:1024190429920>
- 580 González-Soriano, J., Marín García, P., Contreras-Rodríguez, J., Martínez-Sainz, P., & Rodríguez-Veiga, E.  
581 (2001). Age-related changes in the ventricular system of the dog brain. *Annals of Anatomy =*  
582 *Anatomischer Anzeiger: Official Organ of the Anatomische Gesellschaft*, 183(3), 283–291.  
583 [https://doi.org/10.1016/S0940-9602\(01\)80236-3](https://doi.org/10.1016/S0940-9602(01)80236-3)
- 584 Gross, B., Garcia-Tapia, D., Riedesel, E., Ellinwood, N. M., & Jens, J. K. (2010). NORMAL CANINE BRAIN  
585 MATURATION AT MAGNETIC RESONANCE IMAGING: MRI Appearance of Normal Postnatal  
586 Canine Brain Maturation with Histology Correlation. *Veterinary Radiology & Ultrasound*, 51(4),  
587 361–373. <https://doi.org/10.1111/j.1740-8261.2010.01681.x>
- 588 Gunde, E., Czeibert, K., Gábor, A., Szabó, D., Kis, A., Arany-Tóth, A., Andics, A., Gácsi, M., & Kubinyi, E.  
589 (2020). Longitudinal Volumetric Assessment of Ventricular Enlargement in Pet Dogs Trained for  
590 Functional Magnetic Resonance Imaging (fMRI) Studies. *Veterinary Sciences*, 7(3), 127.  
591 <https://doi.org/10.3390/vetsci7030127>
- 592 Hackler, L., Gyuris, M., Huzián, O., Alföldi, R., Szebeni, G. J., Madácsi, R., Knapp, L., Kanizsai, I., & Puskás,  
593 L. G. (2019). Enantioselective Synthesis of 8-Hydroxyquinoline Derivative, Q134 as a Hypoxic  
594 Adaptation Inducing Agent. *Molecules*, 24(23), Article 23.  
595 <https://doi.org/10.3390/molecules24234269>
- 596 Head, E., Callahan, H., Muggenburg, B. A., Cotman, C. W., & Milgram, N. W. (1998). Visual-discrimination  
597 learning ability and beta-amyloid accumulation in the dog. *Neurobiology of Aging*, 19(5), 415–  
598 425. [https://doi.org/10.1016/s0197-4580\(98\)00084-0](https://doi.org/10.1016/s0197-4580(98)00084-0)
- 599 Head, E., McCleary, R., Hahn, F. F., Milgram, N. W., & Cotman, C. W. (2000). Region-specific age at onset  
600 of  $\beta$ -amyloid in dogs☆. *Neurobiology of Aging*, 21(1), 89–96. [https://doi.org/10.1016/S0197-4580\(00\)00093-2](https://doi.org/10.1016/S0197-4580(00)00093-2)  
601

- 602 Head, E., Pop, V., Vasilevko, V., Hill, M., Saing, T., Sarsoza, F., Nistor, M., Christie, L.-A., Milton, S., Glabe,  
603 C., Barrett, E., & Cribbs, D. (2008). A Two-Year Study with Fibrillar  $\beta$ -Amyloid (A $\beta$ ) Immunization  
604 in Aged Canines: Effects on Cognitive Function and Brain A $\beta$ . *The Journal of Neuroscience*,  
605 28(14), 3555–3566. <https://doi.org/10.1523/JNEUROSCI.0208-08.2008>
- 606 Hudry, E., Wu, H.-Y., Arbel-Ornath, M., Hashimoto, T., Matsouaka, R., Fan, Z., Spires-Jones, T. L.,  
607 Betensky, R. A., Bacskai, B. J., & Hyman, B. T. (2012). Inhibition of the NFAT pathway alleviates  
608 amyloid  $\beta$  neurotoxicity in a mouse model of Alzheimer's disease. *The Journal of Neuroscience:*  
609 *The Official Journal of the Society for Neuroscience*, 32(9), 3176–3192.  
610 <https://doi.org/10.1523/JNEUROSCI.6439-11.2012>
- 611 Johnson, P. J., Luh, W.-M., Rivard, B. C., Graham, K. L., White, A., FitzMaurice, M., Loftus, J. P., & Barry, E.  
612 F. (2020). Stereotactic Cortical Atlas of the Domestic Canine Brain. *Scientific Reports*, 10(1),  
613 4781. <https://doi.org/10.1038/s41598-020-61665-0>
- 614 Kim, T. A., Chen, L., & Ge, S. (2021). The Interplay of Neurovasculature and Adult Hippocampal  
615 Neurogenesis. *Neuroscience Letters*, 760, 136071. <https://doi.org/10.1016/j.neulet.2021.136071>
- 616 Kimotsuki, T., Nagaoka, T., Yasuda, M., Tamahara, S., Matsuki, N., & Ono, K. (2005). Changes of Magnetic  
617 Resonance Imaging on the Brain in Beagle Dogs with Aging. *Journal of Veterinary Medical*  
618 *Science*, 67(10), 961–967. <https://doi.org/10.1292/jvms.67.961>
- 619 Kuchibhotla, K. V., Goldman, S. T., Lattarulo, C. R., Wu, H.-Y., Hyman, B. T., & Bacskai, B. J. (2008). Abeta  
620 plaques lead to aberrant regulation of calcium homeostasis in vivo resulting in structural and  
621 functional disruption of neuronal networks. *Neuron*, 59(2), 214–225.  
622 <https://doi.org/10.1016/j.neuron.2008.06.008>
- 623 Lista, S., Dubois, B., & Hampel, H. (2015). Paths to Alzheimer's disease prevention: From modifiable risk  
624 factors to biomarker enrichment strategies. *The Journal of Nutrition, Health & Aging*, 19(2),  
625 154–163. <https://doi.org/10.1007/s12603-014-0515-3>
- 626 London, E. D., Ohata, M., Takei, H., French, A. W., & Rapoport, S. I. (1983). Regional cerebral metabolic  
627 rate for glucose in beagle dogs of different ages. *Neurobiology of Aging*, 4(2), 121–126.  
628 [https://doi.org/10.1016/0197-4580\(83\)90035-0](https://doi.org/10.1016/0197-4580(83)90035-0)
- 629 Maass, A., Düzel, S., Goerke, M., Becke, A., Sobieray, U., Neumann, K., Lövdén, M., Lindenberger, U.,  
630 Bäckman, L., Braun-Dullaeus, R., Ahrens, D., Heinze, H.-J., Müller, N. G., & Düzel, E. (2015).  
631 Vascular hippocampal plasticity after aerobic exercise in older adults. *Molecular Psychiatry*,  
632 20(5), 585–593. <https://doi.org/10.1038/mp.2014.114>
- 633 Martinez, M. N., Mochel, J. P., Neuhoff, S., & Pade, D. (2021). Comparison of Canine and Human  
634 Physiological Factors: Understanding Interspecies Differences that Impact Drug  
635 Pharmacokinetics. *The AAPS Journal*, 23(3), 59. <https://doi.org/10.1208/s12248-021-00590-0>
- 636 Mendez Colmenares, A., Voss, M. W., Fanning, J., Salerno, E. A., Gothe, N. P., Thomas, M. L., McAuley, E.,  
637 Kramer, A. F., & Burzynska, A. Z. (2021). White matter plasticity in healthy older adults: The  
638 effects of aerobic exercise. *NeuroImage*, 239, 118305.  
639 <https://doi.org/10.1016/j.neuroimage.2021.118305>

- 640 Milgram, N. W., Adams, B., Callahan, H., Head, E., Mackay, B., Thirlwell, C., & Cotman, C. W. (1999).  
641 Landmark Discrimination Learning in the Dog. *Learning & Memory*, 6(1), 54–61.
- 642 Milne, M. E., Steward, C., Firestone, S. M., Long, S. N., O'Brien, T. J., & Moffat, B. A. (2016). Development  
643 of representative magnetic resonance imaging–based atlases of the canine brain and evaluation  
644 of three methods for atlas-based segmentation. *American Journal of Veterinary Research*, 77(4),  
645 395–403. <https://doi.org/10.2460/ajvr.77.4.395>
- 646 Minoshima, S., Giordani, B., Berent, S., Frey, K. A., Foster, N. L., & Kuhl, D. E. (1997). Metabolic reduction  
647 in the posterior cingulate cortex in very early Alzheimer's disease. *Annals of Neurology*, 42(1),  
648 85–94. <https://doi.org/10.1002/ana.410420114>
- 649 Niemann, C., Godde, B., Staudinger, U. M., & Voelcker-Rehage, C. (2014). Exercise-induced changes in  
650 basal ganglia volume and cognition in older adults. *Neuroscience*, 281, 147–163.  
651 <https://doi.org/10.1016/j.neuroscience.2014.09.033>
- 652 Norris, C. M., Kadish, I., Blalock, E. M., Chen, K.-C., Thibault, V., Porter, N. M., Landfield, P. W., & Kraner,  
653 S. D. (2005). Calcineurin Triggers Reactive/Inflammatory Processes in Astrocytes and Is  
654 Upregulated in Aging and Alzheimer's Models. *The Journal of Neuroscience*, 25(18), 4649–4658.  
655 <https://doi.org/10.1523/JNEUROSCI.0365-05.2005>
- 656 O'Brien, R. M. (2017). Mixed models, linear dependency, and identification in age-period-cohort models:  
657 Mixed Models and Identification in Age-Period-Cohort Models. *Statistics in Medicine*, 36(16),  
658 2590–2600. <https://doi.org/10.1002/sim.7305>
- 659 Palmqvist, S., Schöll, M., Strandberg, O., Mattsson, N., Stomrud, E., Zetterberg, H., Blennow, K., Landau,  
660 S., Jagust, W., & Hansson, O. (2017). Earliest accumulation of  $\beta$ -amyloid occurs within the  
661 default-mode network and concurrently affects brain connectivity. *Nature Communications*,  
662 8(1), Article 1. <https://doi.org/10.1038/s41467-017-01150-x>
- 663 Pengas, G., Hodges, J. R., Watson, P., & Nestor, P. J. (2010). Focal posterior cingulate atrophy in incipient  
664 Alzheimer's disease. *Neurobiology of Aging*, 31(1), 25–33.  
665 <https://doi.org/10.1016/j.neurobiolaging.2008.03.014>
- 666 Perl, D. P. (2010). Neuropathology of Alzheimer's Disease. *The Mount Sinai Journal of Medicine, New*  
667 *York*, 77(1), 32–42. <https://doi.org/10.1002/msj.20157>
- 668 Pop, V., Head, E., Berchtold, N. C., Glabe, C. G., Studzinski, C. M., Weidner, A. M., Murphy, M. P., &  
669 Cotman, C. W. (2012). A $\beta$  aggregation profiles and shifts in APP processing favor  
670 amyloidogenesis in canines. *Neurobiology of Aging*, 33(1), 108–120.  
671 <https://doi.org/10.1016/j.neurobiolaging.2010.02.008>
- 672 Radhakrishnan, H., Bennett, I. J., & Stark, C. E. (2022). Higher-order multi-shell diffusion measures  
673 complement tensor metrics and volume in gray matter when predicting age and cognition.  
674 *NeuroImage*, 253, 119063. <https://doi.org/10.1016/j.neuroimage.2022.119063>
- 675 Radhakrishnan, H., Ubele, M. F., Krumholz, S. M., Boaz, K., Mefford, J. L., Jones, E. D., Meacham, B.,  
676 Smiley, J., Puskás, L. G., Powell, D. K., Norris, C. M., Stark, C. E. L., & Head, E. (2021). Tacrolimus

- 677 Protects against Age-Associated Microstructural Changes in the Beagle Brain. *Journal of*  
678 *Neuroscience*, 41(23), 5124–5133. <https://doi.org/10.1523/JNEUROSCI.0361-21.2021>
- 679 Rajan, K. B., Weuve, J., Barnes, L. L., McAninch, E. A., Wilson, R. S., & Evans, D. A. (2021). Population  
680 Estimate of People with Clinical AD and Mild Cognitive Impairment in the United States (2020–  
681 2060). *Alzheimer's & Dementia : The Journal of the Alzheimer's Association*, 17(12), 1966–1975.  
682 <https://doi.org/10.1002/alz.12362>
- 683 Randhawa, P. S., Starzl, T. E., & Demetris, A. J. (1997). Tacrolimus (FK506)-Associated Renal Pathology.  
684 *Advances in Anatomic Pathology*, 4(4), 265–276.
- 685 Raz, N., Ghisletta, P., Rodrigue, K. M., Kennedy, K. M., & Lindenberger, U. (2010). Trajectories of brain  
686 aging in middle-aged and older adults: Regional and individual differences. *NeuroImage*, 51(2),  
687 501–511. <https://doi.org/10.1016/j.neuroimage.2010.03.020>
- 688 Raz, N., Rodrigue, K. M., Kennedy, K. M., Head, D., Gunning-Dixon, F., & Acker, J. D. (2003). Differential  
689 Aging of the Human Striatum: Longitudinal Evidence. *American Journal of Neuroradiology*, 24(9),  
690 1849–1856.
- 691 Reese, L. C., & Tagliatela, G. (2010). Neuroimmunomodulation by Calcineurin in Aging and Alzheimer's  
692 Disease. *Aging and Disease*, 1(3), 245–253.
- 693 Rofina, J. E., van Ederen, A. M., Toussaint, M. J. M., Secrève, M., van der Spek, A., van der Meer, I., Van  
694 Eerdenburg, F. J. C. M., & Gruys, E. (2006). Cognitive disturbances in old dogs suffering from the  
695 canine counterpart of Alzheimer's disease. *Brain Research*, 1069(1), 216–226.  
696 <https://doi.org/10.1016/j.brainres.2005.11.021>
- 697 Scheff, S. W., & Price, D. A. (2001). Alzheimer's disease-related synapse loss in the cingulate cortex.  
698 *Journal of Alzheimer's Disease: JAD*, 3(5), 495–505. <https://doi.org/10.3233/jad-2001-3509>
- 699 Scheff, S. W., Price, D. A., Ansari, M. A., Roberts, K. N., Schmitt, F. A., Ikonomic, M. D., & Mufson, E. J.  
700 (2015). Synaptic change in the posterior cingulate gyrus in the progression of Alzheimer's  
701 disease. *Journal of Alzheimer's Disease: JAD*, 43(3), 1073–1090. [https://doi.org/10.3233/JAD-](https://doi.org/10.3233/JAD-141518)  
702 141518
- 703 Scholz, J., Klein, M. C., Behrens, T. E., & Johansen-Berg, H. (2009). Training induces changes in white-  
704 matter architecture. *Nature Neuroscience*, 12(11), 1370–1371.
- 705 Siwak-Tapp, C. T., Head, E., Muggenburg, B. A., Milgram, N. W., & Cotman, C. W. (2008). Region specific  
706 neuron loss in the aged canine hippocampus is reduced by enrichment. *Neurobiology of Aging*,  
707 29(1), 39–50. <https://doi.org/10.1016/j.neurobiolaging.2006.09.018>
- 708 Sompol, P., Furman, J. L., Pleiss, M. M., Kraner, S. D., Artiushin, I. A., Batten, S. R., Quintero, J. E.,  
709 Simmerman, L. A., Beckett, T. L., Lovell, M. A., Murphy, M. P., Gerhardt, G. A., & Norris, C. M.  
710 (2017). Calcineurin/NFAT Signaling in Activated Astrocytes Drives Network Hyperexcitability in  
711 A $\beta$ -Bearing Mice. *The Journal of Neuroscience*, 37(25), 6132–6148.  
712 <https://doi.org/10.1523/JNEUROSCI.0877-17.2017>

- 713 Sompol, P., Gollihue, J. L., Kraner, S. D., Artiushin, I. A., Cloyd, R. A., Chishti, E. A., Koren, S. A., Nation, G.  
714 K., Abisambra, J. F., Huzian, O., Nagy, L. I., Santha, M., Hackler, L., Puskas, L. G., & Norris, C. M.  
715 (2021). Q134R: Small chemical compound with NFAT inhibitory properties improves behavioral  
716 performance and synapse function in mouse models of amyloid pathology. *Aging Cell*, *20*(7),  
717 e13416. <https://doi.org/10.1111/accel.13416>
- 718 Song, Z., Krishnan, A., Gaetano, L., Tustison, N. J., Clayton, D., de Crespigny, A., Bengtsson, T., Jia, X., &  
719 Carano, R. A. D. (2022). Deformation-based morphometry identifies deep brain structures  
720 protected by ocrelizumab. *NeuroImage: Clinical*, *34*, 102959.  
721 <https://doi.org/10.1016/j.nicl.2022.102959>
- 722 Stallings, N. R., O'Neal, M. A., Hu, J., Shen, Z.-J., & Malter, J. S. (2023). Long-term normalization of  
723 calcineurin activity in model mice rescues Pin1 and attenuates Alzheimer's phenotypes without  
724 blocking peripheral T cell IL-2 response. *Alzheimer's Research & Therapy*, *15*(1), 179.  
725 <https://doi.org/10.1186/s13195-023-01323-5>
- 726 Studzinski, C., Christie, L., Araujo, J., Burnham, W., Head, E., Cotman, C., & Milgram, N. (2006).  
727 Visuospatial function in the beagle dog: An early marker of cognitive decline in a model of  
728 human aging and dementia. *Neurobiology of Learning and Memory*, *86*(2), 197–204.  
729 <https://doi.org/10.1016/j.nlm.2006.02.005>
- 730 Su, M.-Y., Head, E., Brooks, W. M., Wang, Z., Muggenburg, B. A., Adam, G. E., Sutherland, R., Cotman, C.  
731 W., & Nalcioğlu, O. (1998). Magnetic resonance imaging of anatomic and vascular characteristics  
732 in a canine model of human aging. *Neurobiology of Aging*, *19*(5), 479–485.  
733 [https://doi.org/10.1016/S0197-4580\(98\)00081-5](https://doi.org/10.1016/S0197-4580(98)00081-5)
- 734 Su, M.-Y., Tapp, P. D., Vu, L., Chen, Y.-F., Chu, Y., Muggenburg, B., Chiou, J.-Y., Chen, C., Wang, J., Bracco,  
735 C., & Head, E. (2005). A longitudinal study of brain morphometrics using serial magnetic  
736 resonance imaging analysis in a canine model of aging. *Progress in Neuro-Psychopharmacology  
737 and Biological Psychiatry*, *29*(3), 389–397. <https://doi.org/10.1016/j.pnpbp.2004.12.005>
- 738 Tagliatela, G., Hogan, D., Zhang, W.-R., & Dineley, K. T. (2009). Intermediate- and long-term  
739 recognition memory deficits in Tg2576 mice are reversed with acute calcineurin inhibition.  
740 *Behavioural Brain Research*, *200*(1), 95–99. <https://doi.org/10.1016/j.bbr.2008.12.034>
- 741 Tagliatela, G., Rastellini, C., & Cicalese, L. (2015). Reduced Incidence of Dementia in Solid Organ  
742 Transplant Patients Treated with Calcineurin Inhibitors. *Journal of Alzheimer's Disease*, *47*(2),  
743 329–333. <https://doi.org/10.3233/JAD-150065>
- 744 Tapp, P. D., Head, K., Head, E., Milgram, N. W., Muggenburg, B. A., & Su, M.-Y. (2006). Application of an  
745 automated voxel-based morphometry technique to assess regional gray and white matter brain  
746 atrophy in a canine model of aging. *NeuroImage*, *29*(1), 234–244.  
747 <https://doi.org/10.1016/j.neuroimage.2005.07.043>
- 748 Tapp, P. D., Siwak, C. T., Estrada, J., Head, E., Muggenburg, B. A., Cotman, C. W., & Milgram, N. W.  
749 (2003). Size and Reversal Learning in the Beagle Dog as a Measure of Executive Function and  
750 Inhibitory Control in Aging. *Learning & Memory*, *10*(1), 64–73. <https://doi.org/10.1101/lm.54403>

751 Tapp, P. D., Siwak, C. T., Gao, F. Q., Chiou, J.-Y., Black, S. E., Head, E., Muggenburg, B. A., Cotman, C. W.,  
752 Milgram, N. W., & Su, M.-Y. (2004). Frontal lobe volume, function, and beta-amyloid pathology  
753 in a canine model of aging. *The Journal of Neuroscience: The Official Journal of the Society for*  
754 *Neuroscience*, 24(38), 8205–8213. <https://doi.org/10.1523/JNEUROSCI.1339-04.2004>

755 Tustison, N. J., Avants, B. B., Cook, P. A., Yuanjie Zheng, Egan, A., Yushkevich, P. A., & Gee, J. C. (2010).  
756 N4ITK: Improved N3 Bias Correction. *IEEE Transactions on Medical Imaging*, 29(6), 1310–1320.  
757 <https://doi.org/10.1109/TMI.2010.2046908>

758 Tustison, N. J., Cook, P. A., Holbrook, A. J., Johnson, H. J., Muschelli, J., Devenyi, G. A., Duda, J. T., Das, S.  
759 R., Cullen, N. C., Gillen, D. L., Yassa, M. A., Stone, J. R., Gee, J. C., & Avants, B. B. (2021). The  
760 ANTsX ecosystem for quantitative biological and medical imaging. *Scientific Reports*, 11, 9068.  
761 <https://doi.org/10.1038/s41598-021-87564-6>

762 Tustison, N. J., Cook, P. A., Klein, A., Song, G., Das, S. R., Duda, J. T., Kandel, B. M., van Strien, N., Stone, J.  
763 R., Gee, J. C., & Avants, B. B. (2014). Large-scale evaluation of ANTs and FreeSurfer cortical  
764 thickness measurements. *Neuroimage*, 99, 166–179.  
765 <https://doi.org/10.1016/j.neuroimage.2014.05.044>

766 Tustison, N. J., Holbrook, A. J., Avants, B. B., Roberts, J. M., Cook, P. A., Reagh, Z. M., Duda, J. T., Stone, J.  
767 R., Gillen, D. L., & Yassa, M. A. (2019). Longitudinal Mapping of Cortical Thickness  
768 Measurements: An Alzheimer’s Disease Neuroimaging Initiative-Based Evaluation Study. *Journal*  
769 *of Alzheimer’s Disease*, 71(1), 165–183. <https://doi.org/10.3233/JAD-190283>

770 Vite, C. H., & Head, E. (2014). Aging in the Canine and Feline Brain. *Veterinary Clinics of North America:*  
771 *Small Animal Practice*, 44(6), 1113–1129. <https://doi.org/10.1016/j.cvsm.2014.07.008>

772 Yu, Z., Guindani, M., Grieco, S. F., Chen, L., Holmes, T. C., & Xu, X. (2022). Beyond t test and ANOVA:  
773 Applications of mixed-effects models for more rigorous statistical analysis in neuroscience  
774 research. *Neuron*, 110(1), 21–35. <https://doi.org/10.1016/j.neuron.2021.10.030>

775 Yu, Z., Han, X., Xu, W., Zhang, J., Marr, C., Shen, D., Peng, T., Zhang, X.-Y., & Feng, J. (2022). A  
776 generalizable brain extraction net (BEN) for multimodal MRI data from rodents, nonhuman  
777 primates, and humans. *eLife*, 11, e81217. <https://doi.org/10.7554/eLife.81217>

778

779

780

781

782

783

784

785

786

787

<i>Group</i>	<i>N</i>	<i>Age at Start</i>	<i>Sex</i>
<i>Placebo</i>	14	6.23 ± 0.95	12F, 2M
<i>Tacrolimus</i>	15	6.64 ± 1.34	13F, 2M
<i>Q134R</i>	14	6.53 ± 1.12	11F, 3M

Table 1. Dog characteristics. Ages are presented as mean ± standard deviation (SD).

JNeurosci Accepted Manuscript

788

789

<i>ROI</i>	<i>Lobe</i>	<i>T0 volume ± SD (mm<sup>3</sup>)</i>
1. Orbital gyrus	Frontal	652.48 ± 70.75
2. Pregenua gyrus	Frontal	225.86 ± 21.69
3. Gyrus proreus	Frontal	235.91 ± 49.63
4. Anterior compositus gyrus	Sensory-motor	727.67 ± 76.88
5. Precruciate	Sensory-motor	547.19 ± 68.59
6. Genualis	Cingulate	146.08 ± 16.65
7. Anterior cingulate gyrus	Cingulate	108.95 ± 9.91
8. Medial cingulate gyrus	Cingulate	118.43 ± 11.73
9. Posterior cingulate gyrus	Cingulate	375.43 ± 36.94
10. Medial occipital gyrus	Occipital	1163.82 ± 108.14
11. Recurrens	Occipital	192.04 ± 30.91
12. Pararecurrens	Occipital	211.77 ± 24.82
13. Suprasylvian gyrus	Occipital	1285.17 ± 148.69
14. Lateral fissure	Occipital	233.51 ± 29.37
15. Coronal gyrus	Parietal	230.87 ± 31.41
16. Presplenial gyrus	Parietal	170.29 ± 17.94
17. Entolateral gyrus	Parietal	459.11 ± 73.22
18. Marginal gyrus	Parietal	230.55 ± 22.68
19. Posterior compositus gyrus	Temporal	594.14 ± 69.97
20. Ectosylvian gyrus	Temporal	1677.71 ± 162.77
21. Sylvian gyrus	Temporal	1027.48 ± 108.43
22. Amygdala	Subcortical	124.57 ± 11.86
23. Caudate nucleus	Subcortical	483.14 ± 44.38
24. Hippocampus	Subcortical	520.39 ± 50.12

790 Table 2. ROIs from the simplified Johnson atlas, lobar locations, and mean volume (mm<sup>3</sup>) ± SD at the  
791 baseline scan (T0).

Region	Lobe	Median Slope	IQR	Median Rank	Rank IQR
Orbital	Frontal	- 0.164937	952	5	6
Pregenua	Frontal	- 0.152602	518	6	8.5
Proreus	Frontal	- 0.21141	111	5	10.5
Anterior Cingulate	Cingulate	- 0.114573	79	10	8
Precuneate	Sensory-Motor	- 0.138192	43	8	9.5
Genualis	Cingulate	- 0.000712	686	17	8.5
Anterior Compositus	Sensory-Motor	- 0.121159	34	10	11
Medial Cingulate	Cingulate	- 0.070759	147	13	10
Posterior Cingulate	Cingulate	- 0.121226	78	10	9
Medial Occipital	Occipital	- 0.077765	8	14	6
Recurrens	Occipital	- 0.163141	954	11	13
Pararecurrens	Occipital	- 0.117539	721	8	13.5
Suprasylvian	Occipital	- 0.043906	33	17	6.5
Lateral Fissure	Occipital	- 0.051082	909	15	9.5
PRCoronal	Parietal	- 0.01843	906	16	6.5

Presplenial	Parietal	- 0.100011	541	0.160	12	9. 5
Entolateral	Parietal	0.014 479	597	0.177	18	10
PRMarginal	Parietal	- 0.101112	757	0.211	11	10
Posterior Compositus	Tempor al	- 0.180458	34	0.152	6	6. 5
Ectosylvian	Tempor al	- 0.072358	968	0.097	14	4
Sylvian	Tempor al	- 0.142836	467	0.093	8	5. 5
Amygdala	Subcort ical	- 0.008197	339	0.139	17	10
Caudate Nucleus	Subcort ical	0.055 629	977	0.133	22	4. 5
Hippocamp us	Subcort ical	0.157 849	843	0.110	24	2

794 **Table 3.** Median volume-over-time slope and ranks for the slopes for each ROI. IQR=inter-quartile range.

795

Region	tstat	pval	pval_adjusted
Orbital	- 7.787373	<0.0001	<0.0001
Pregenua	- 7.875295	<0.0001	<0.0001
Proreus	-5.76593	<0.0001	<0.0001
AnteriorCompositus	-3.49838	0.0011	0.0088
Precruciate	- 6.375448	<0.0001	<0.0001
Genualis	- 0.290519	0.7728	0.9713
AnteriorCingulate	- 5.889655	<0.0001	<0.0001
MedialCingulate	- 4.065612	0.0002	0.0022
PosteriorCingulate	- 5.035147	<0.0001	<0.0001
MedialOccipital	- 5.444237	<0.0001	<0.0001
Recurrans	- 5.300234	<0.0001	<0.0001
Pararecurrans	- 6.048501	<0.0001	<0.0001
Suprasylvian	0.019072	0.9849	0.9849
LateralFissure	- 3.689741	0.0006	0.0054
PRCoronal	- 0.567065	0.5737	0.967
Presplenial	-4.96738	<0.0001	<0.0001
Entolateral	0.768581	0.4464	0.948

PRMarginal	- 2.767238	0.0084	0.0494
PosteriorCompositus	- 8.246205	<0.0001	<0.0001
Ectosylvian	- 3.211701	0.0025	0.0174
Sylvian	- 8.558256	<0.0001	<0.0001
Amygdala	- 0.396209	0.694	0.9713
CaudateNucleus	4.093335	0.0002	0.0022
Hippocampus	7.447361	<0.0001	<0.0001

797 **Table 4.** One-sample t-tests against zero for each set of dog-specific volume slopes of each ROI. The  
798 Holm-Sidak method was used for adjusting p-values for multiple comparisons.

799

Estimate	Coef.	Std. Err.	z	P	[	0
			> z	0.025	.975]	
Intercept	.088	.131	.668	.504	0.17	.345
Region[T.Amygdala]	-.089	.133	-.67	.503	0.35	.172
Region[T.AnteriorCingulate]	.016	.133	.122	.903	0.245	.277
Region[T.AnteriorCompositus]	.03	.133	.226	.821	0.231	.291
Region[T.CaudateNucleus]	.015	.133	.112	.911	0.246	.276
Region[T.Ectosylvian]	.01	.133	.075	.94	0.251	.271
Region[T.Entolateral]	.003	.133	.02	.984	0.258	.264
Region[T.Genualis]	.078	.133	.583	.56	0.183	.339
Region[T.LateralFissure]	-.114	.133	-.853	.394	0.375	.147
Region[T.MedialCingulate]	.019	.133	.139	.889	0.242	.279
Region[T.MedialOccipital]	-.071	.133	-.536	.592	0.332	.19
Region[T.Orbital]	-.045	.133	-.338	.735	0.306	.216
Region[T.PRCoronal]	-.01	.133	-.075	.94	0.271	.251
Region[T.PRMarginal]	.018	.133	.139	.89	0.242	.279
Region[T.Pararecurrens]	.155	.133	1.164	.245	0.416	.106

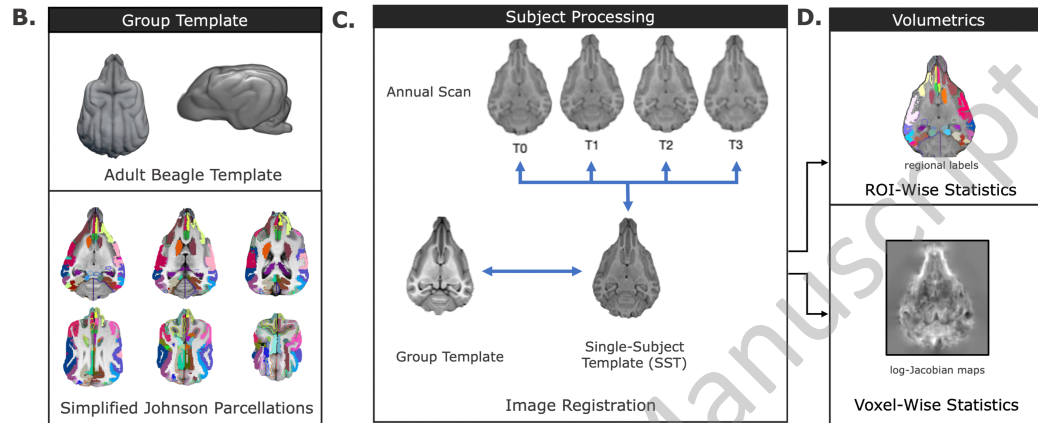
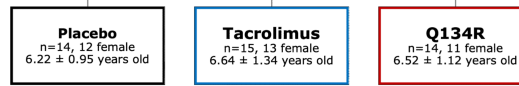
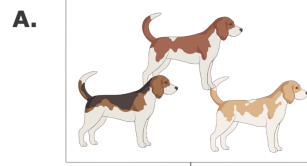
Region[T.PosteriorCingulate]	-	0.	-	0	-	0
	0.029	133	0.216	.829	0.29	.232
Region[T.PosteriorCompositus]	-	0.	-	0	-	0
	0.203	133	1.524	.127	0.464	.058
Region[T.Precruciate]	-	0.	-	0	-	0
	0.063	133	0.476	.634	0.324	.198
Region[T.Pregenua]	-	0.	-	0	-	0
	0.04	133	0.3	.764	0.301	.221
Region[T.Presplenial]	-	0.	-	0	-	0
	0.012	133	0.087	.93	0.273	.249
Region[T.Proreus]	-	0.	-	0	-	0
	0.128	133	0.959	.338	0.389	.133
Region[T.Recurrans]	-	0.	-	0	-	0
	0.183	133	1.376	.169	0.444	.078
Region[T.Suprasylvian]	0	0.	0	0	-	0
	.013	133	.094	.925	0.248	.273
Region[T.Sylvian]	0	0.	-	0	-	0
		133	0.004	.997	0.261	.26
BAge_norm	-	0.	-	0	-	0
	0.144	092	1.558	.119	0.325	.037
Time	0	0.	3	<	0	0
	.181	048	.77	0.001	.087	.275
Time:Region[T.Amygdala]	-	0.	-	0	-	-
	0.188	068	2.774	.006	0.321	0.055
Time:Region[T.AnteriorCingulate]	-	0.	-	<	-	-
	0.299	068	4.415	0.001	0.432	0.166
Time:Region[T.AnteriorCompositus]	-	0.	-	<	-	-
	0.281	068	4.142	0.001	0.414	0.148
Time:Region[T.CaudateNucleus]	-	0.	-	0	-	0
	0.132	068	1.954	.051	0.265	
Time:Region[T.Ectosylvian]	-	0.	-	0	-	-
	0.226	068	3.333	.001	0.359	0.093
Time:Region[T.Entolateral]	-	0.	-	0	-	-
	0.163	068	2.404	.016	0.296	0.03

Time:Region[T.Genua lis]	- 0.189	0. 068	- 2.782	0 .005	- 0.321	- 0.056
Time:Region[T.Latera lFissure]	- 0.248	0. 068	- 3.666	< 0.001	- 0.381	- 0.116
Time:Region[T.Media lCingulate]	- 0.27	0. 068	- 3.987	< 0.001	- 0.403	- 0.137
Time:Region[T.Media lOccipital]	- 0.231	0. 068	- 3.41	0 .001	- 0.364	- 0.098
Time:Region[T.Orbita l]	- 0.355	0. 068	- 5.236	< 0.001	- 0.488	- 0.222
Time:Region[T.PRCor onal]	- 0.196	0. 068	- 2.891	0 .004	- 0.329	- 0.063
Time:Region[T.PRMa rginal]	- 0.254	0. 068	- 3.75	< 0.001	- 0.387	- 0.121
Time:Region[T.Parare currens]	- 0.32	0. 068	- 4.715	< 0.001	- 0.452	- 0.187
Time:Region[T.Poster iorCingulate]	- 0.295	0. 068	- 4.353	< 0.001	- 0.428	- 0.162
Time:Region[T.Poster iorCompositus]	- 0.373	0. 068	- 5.508	< 0.001	- 0.506	- 0.24
Time:Region[T.Precru ciate]	- 0.323	0. 068	- 4.772	< 0.001	- 0.456	- 0.191
Time:Region[T.Prege nual]	- 0.37	0. 068	- 5.46	< 0.001	- 0.503	- 0.237
Time:Region[T.Prespl enial]	- 0.269	0. 068	- 3.972	< 0.001	- 0.402	- 0.136
Time:Region[T.Prore us]	- 0.384	0. 068	- 5.666	< 0.001	- 0.517	- 0.251
Time:Region[T.Recurr ens]	- 0.327	0. 068	- 4.826	< 0.001	- 0.46	- 0.194
Time:Region[T.Supras ylvian]	- 0.178	0. 068	- 2.633	0 .008	- 0.311	- 0.046
Time:Region[T.Sylvia n]	- 0.307	0. 068	- 4.527	< 0.001	- 0.44	- 0.174

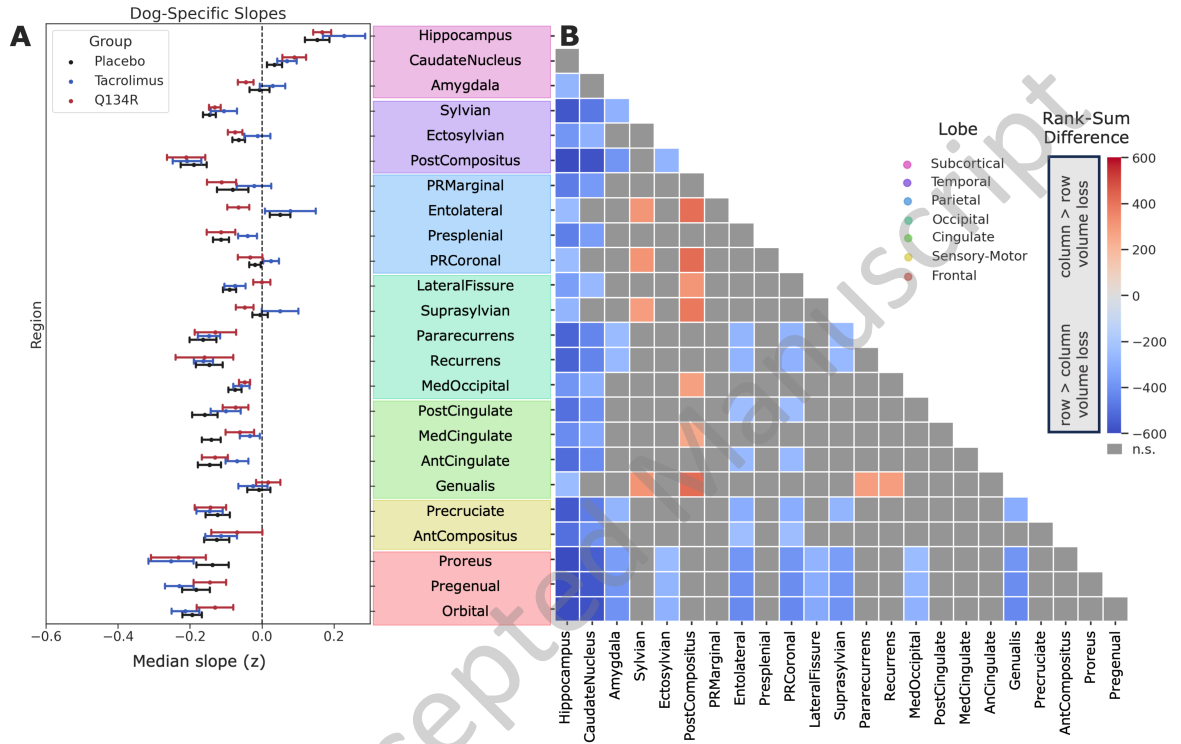
801 **Table 5.** Parameter estimates from the all-ROI-inclusive LME model where the hippocampus was  
802 assigned as the reference level for the “Region” predictor.

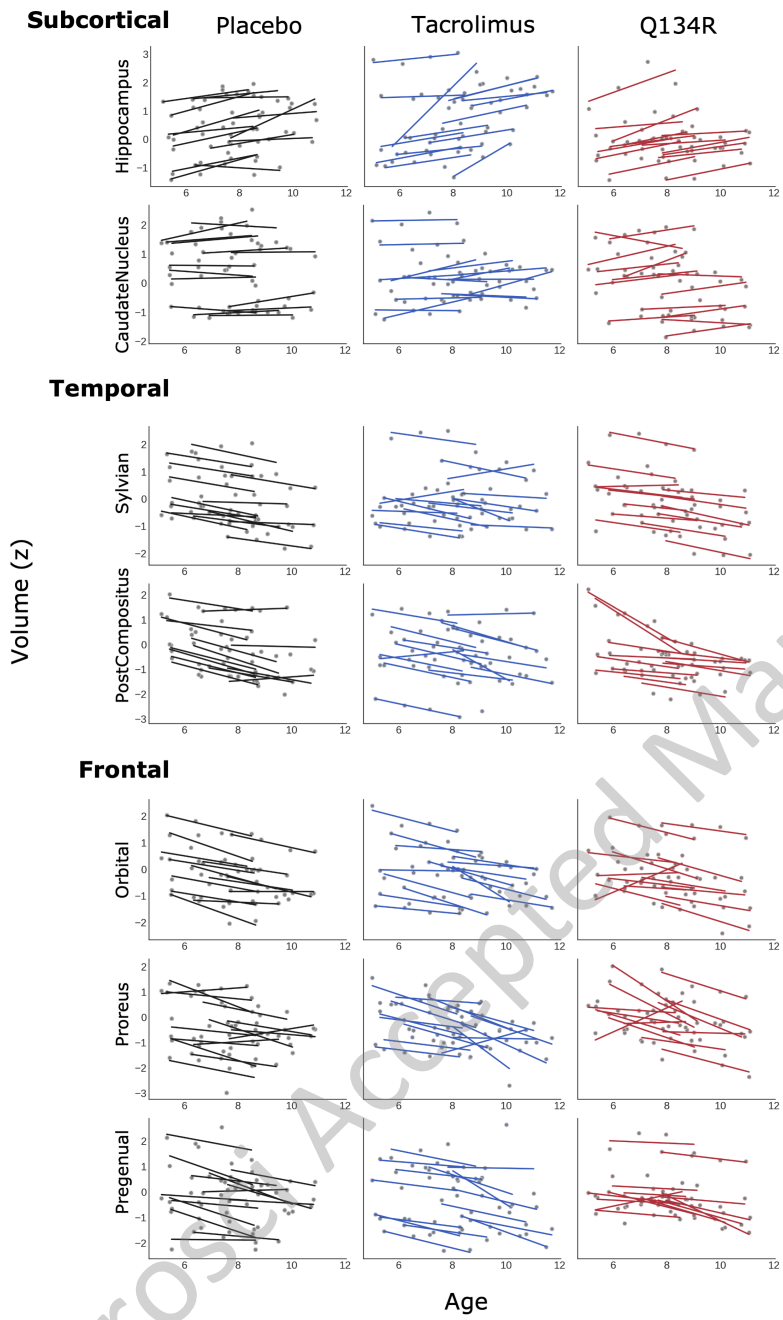
803

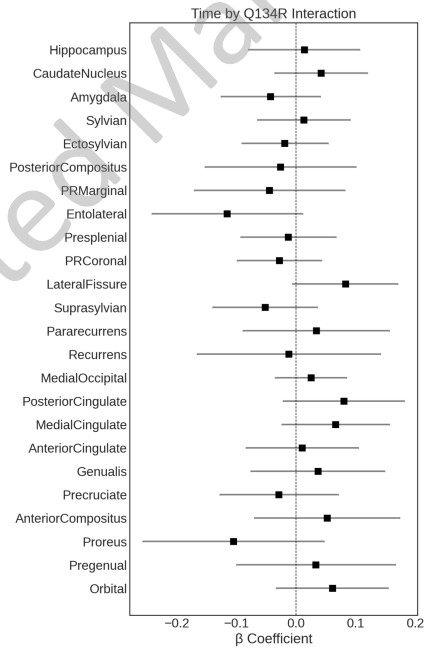
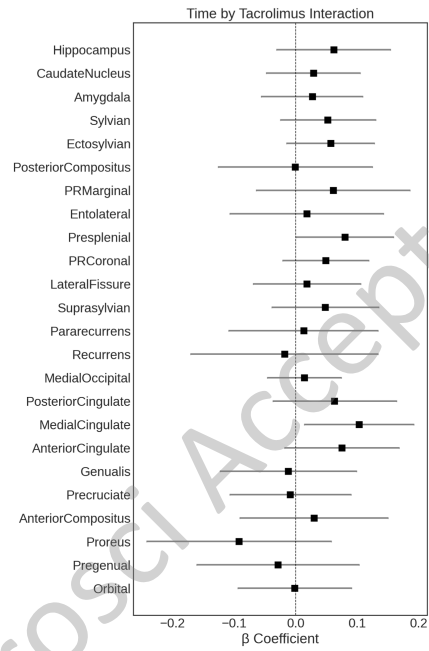
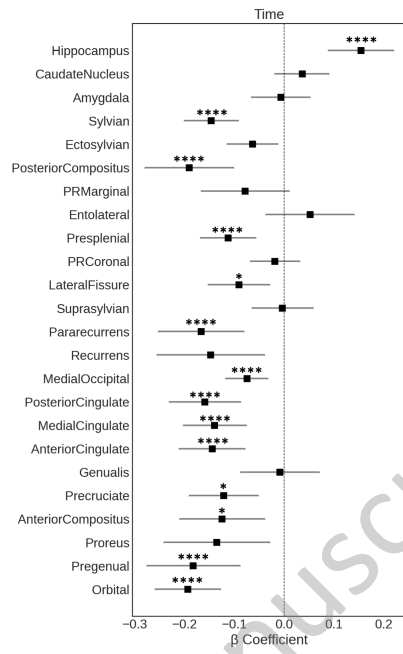
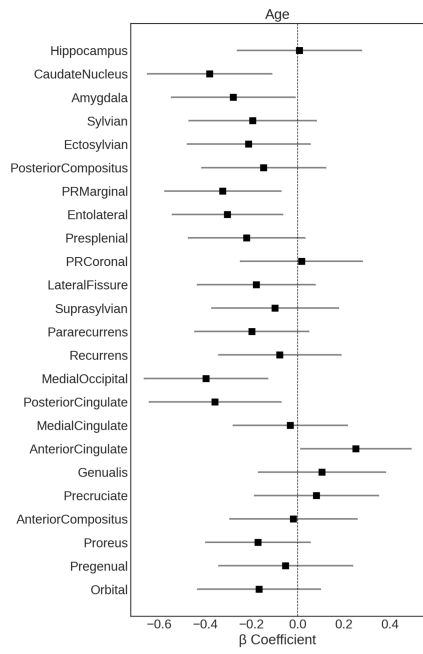
JNeurosci Accepted Manuscript



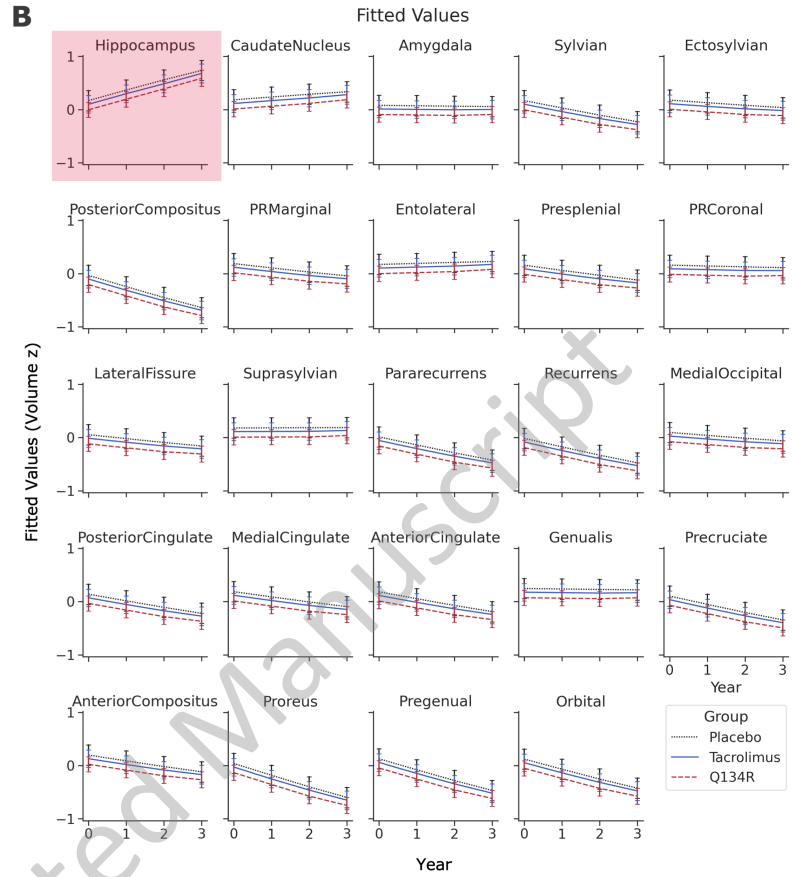
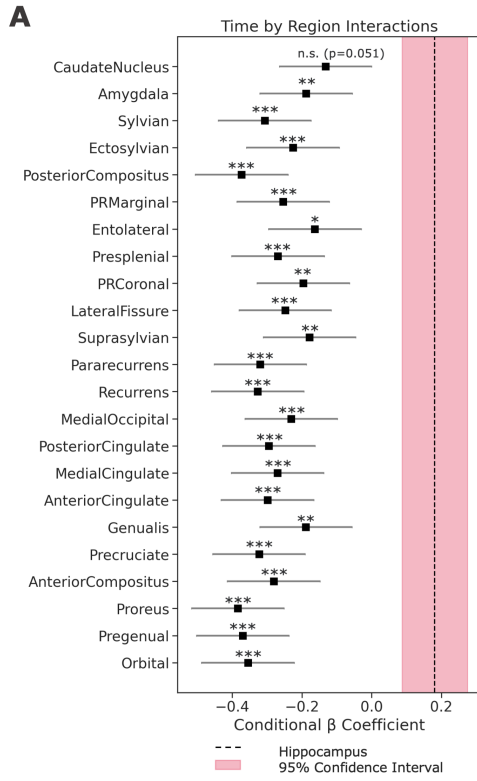
JNeurosci Accepted Manuscript



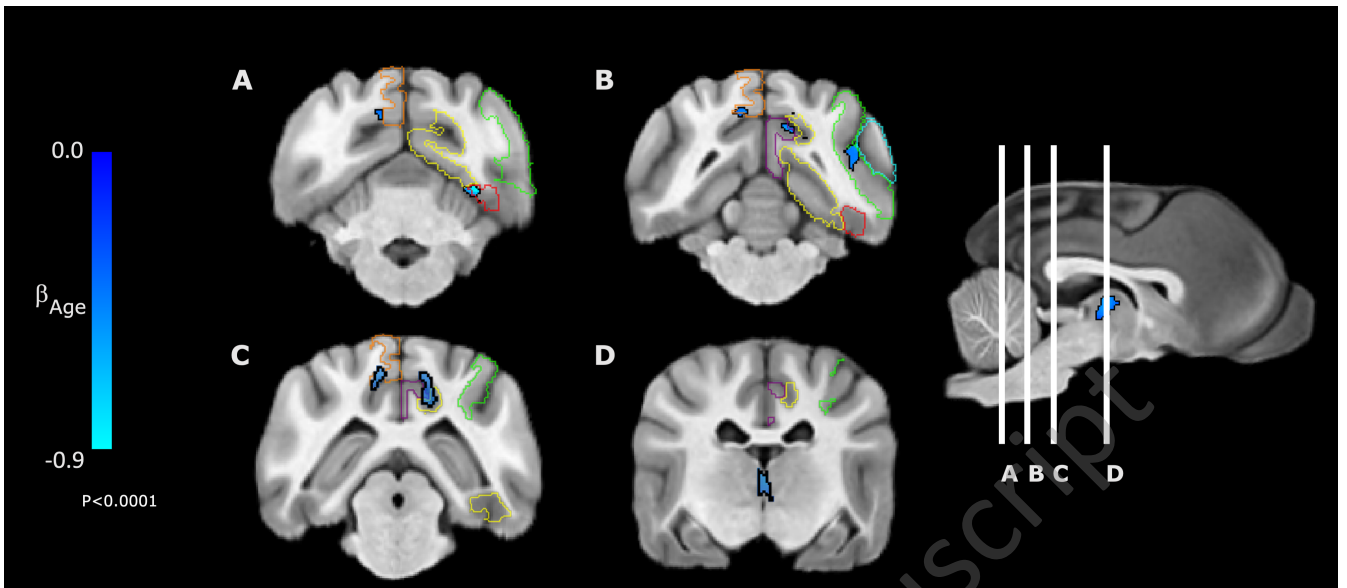




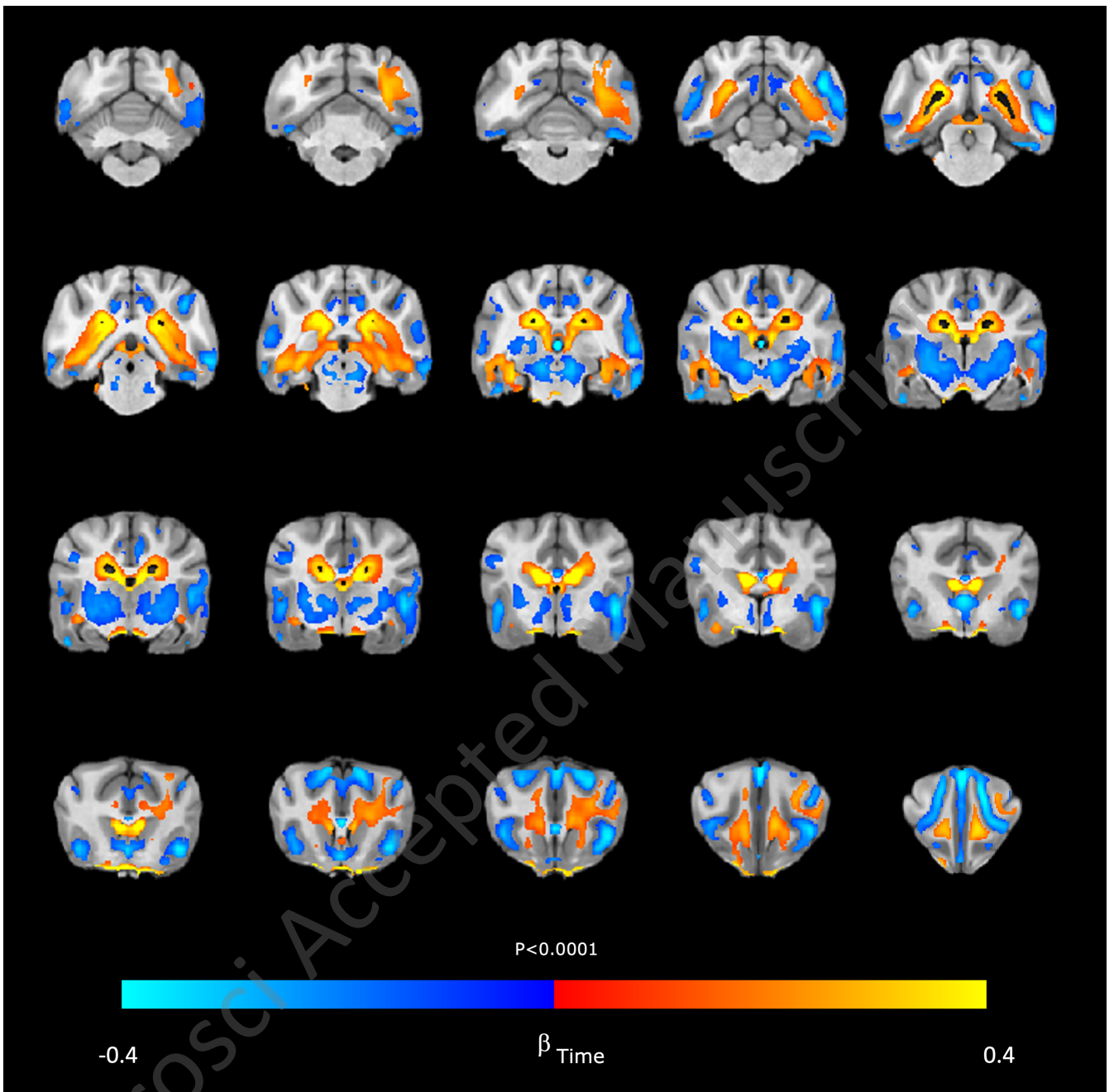
JNeurosci Accepted Manuscript

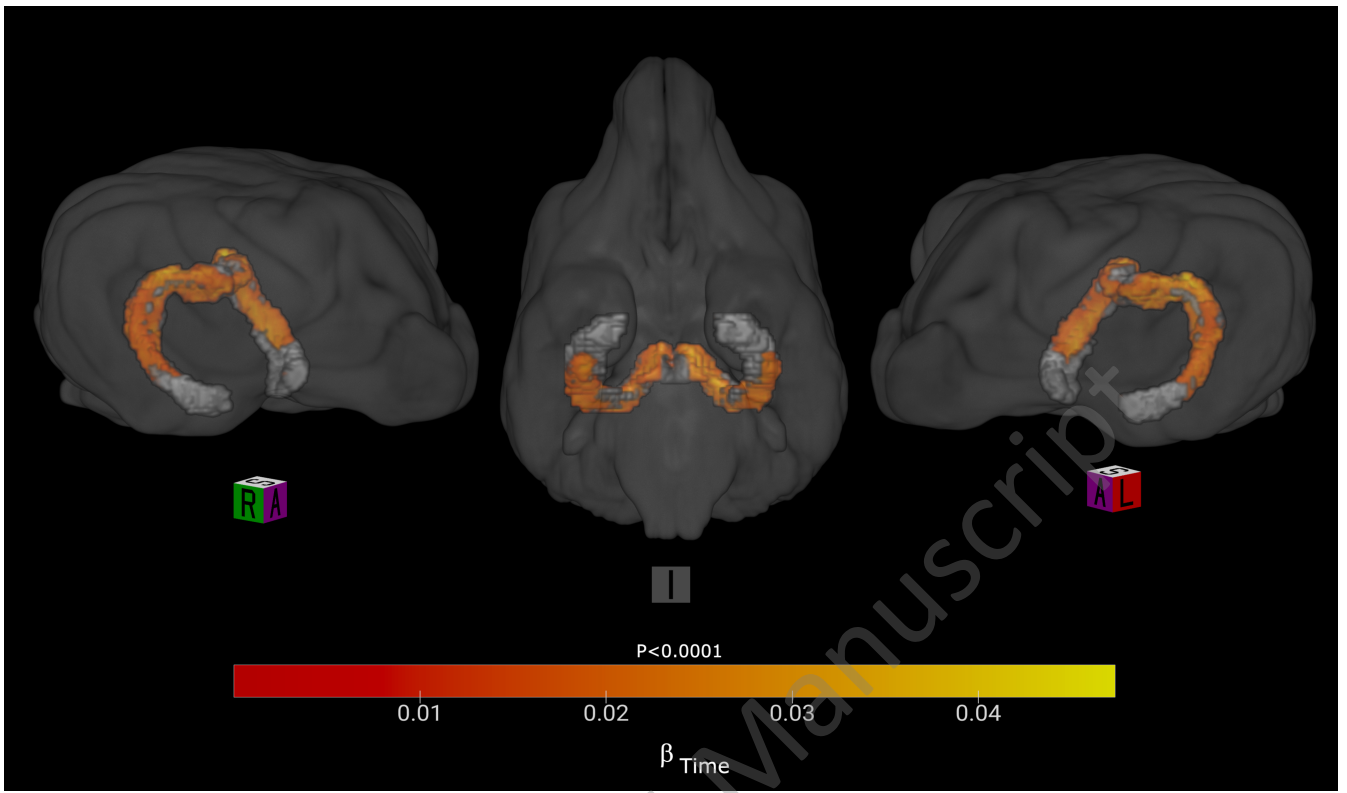


JNeurosci Accepted Manuscript



JNeurosci Accepted Manuscript





JNeurosci Accepted Manuscript

